Conformational properties of comb copolymer brushes: Persistence and Curvature

Johan de Jong

Paranimfen: Dr. A.A.T.S. Reinders
T.R. de Jong, BSW

Typesetting: 11pt Utopia using LaTeX
Printing: Universal press (http://www.uponline.nl)
Cover illustration: comb copolymer displaying intramolecular phase separation and bending (Fig. 4.10E).

Financial support for the publication of this thesis was provided by:
- Materials Science Centre (MSC)
- University of Groningen (RuG)

MSC Ph.D.-thesis series 2005-10
ISSN 1570-1530

Publisher: bibliotheek der RuG
ISBN number: 90-367-2372-8
ISBN electronic: 90-367-2373-6

RIJKSUNIVERSITEIT GRONINGEN

Conformational properties of comb copolymer brushes: Persistence and Curvature

Proefschrift

ter verkrijging van het doctoraat in de
Wiskunde en Natuurwetenschappen
aan de Rijksuniversiteit Groningen
op gezag van de
Rector Magnificus, dr. F. Zwarts,
in het openbaar te verdedigen op
vrijdag 2 december 2005
om 16.15 uur

door

Johannes Rinse de Jong
geboren op 13 juli 1974
te Workum

Promotor:	Prof. Dr. G. ten Brinke
Copromotor:	Dr. A.V. Subbotin
Beoordelingscommissie:	Prof. Dr. P.G. Khalatur Prof. Dr. J.J.M. Slot Prof. Dr. E.L.F. Nies

ISBN: 90-367-2372-8

Voor:

Simone
Heit
Mem
Titia

A mind is like a parachute. It doesn't work if it's not open.

- Frank Zappa

Contents

Contents

Outline

The research reported in this thesis is concerned with the conformational properties of comb copolymer brushes in infinitely dilute solution. In particular the focus is turned towards stiffness and (spontaneous) curvature. The conformational properties of comb copolymer brushes in solvent may be influenced in various ways by designing a particular architecture, using variables such as topology and chemical composition, as well as by imposing certain conditions such as topological constraints, temperature, and solvent conditions.

This thesis consists of two main parts. The first of these provides some background and context to the research topic of this work in the form of three review chapters. The first chapter (Chapter 1) is concerned with the experimental aspects of cylindrical polymer brushes. It focuses mainly on the types of polymer brushes, based on architecture and (chemical) composition, that have been synthesized successfully over the last two decades rather than on the chemical details and the polymerization techniques. Using chemically different types of side chains in the same comb copolymer brush combined with the use of selective solvent it is possible to induce intra-molecular phase separation resulting, e.g. in so-called Janus micelles.

Next, the experimental characterization of the comb copolymer brush conformation in dilute solution is discussed. Using a combination of theoretical modelling and light scattering experiments physical quantities such as the radius of gyration, the Kuhn statistical segment size and the contour length per monomer can be evaluated. The discussion is complemented by an example using simulation data. Particularly noteworthy is the fact that the contour length per monomer is generally much smaller than the all-trans value, demonstrating that the polymer backbone is locally coiled rather than being fully stretched. Another very useful technique is the

visualization of molecular brush conformations by AFM. The observation of spiralling conformations for molecular brushes strongly adsorbed onto a flat substrate has spawned a number of theoretical studies discussing spontaneous curvature. This issue is being addressed in this thesis by computer simulation which will be discussed in Chapter 5. The review is concluded by discussing a number of applications of cylindrical polymer brushes such as molecular valves.

Chapter 2 discusses the theoretical aspects of comb copolymer brushes. It starts with outlining a scaling analysis of a comb copolymer brush having a straight backbone. Here the blob model is introduced and a relation between brush radius, grafting density and side chain length is reproduced. Next the free energy of the comb copolymer brush as a function of bending is calculated in analogy with the original work of Fredrickson. This analysis leads to a prediction on the scaling behavior of the persistence length with respect to grafting density and side chain length. Calculation of the ratio between the persistence length and the brush diameter leads to the prediction that if the side chains are long enough the comb copolymer brush becomes a very stiff object.

Scaling arguments and the blob model are employed to analyze spontaneous curvature of the 2D bottle brush. It is shown that scaling arguments predict the 2D bottle brush to be stable with respect to bending, contrary to the mean field analysis by Potemkin and coworkers. Experiments as well as the computer simulation study presented in Chapter 5 confirm the presence of spontaneous curvature. However, spontaneous curvature did not turn up in previous simulation studies and this matter will be discussed in Chapter 7.

Chapter 3 discusses Monte Carlo simulations on cylindrical polymer brushes. It starts out by giving a general introduction of Monte Carlo simulations and how these can be applied to polymer systems. In particular the bond fluctuation model (BFM) is discussed which has been used in all simulation studies reported in this thesis. In addition the so-called 'infinite lattice' approach is outlined which we developed to get rid of the need for very large simulation boxes such that simulations of large systems can be performed on computers with low memory, thus making it particularly useful for simulations on Beowulf type computer clusters. The chapter proceeds with a discussion of the literature on Monte Carlo simulations of branched polymers.

The second part of this thesis reports our simulation studies on the conformational behavior of comb copolymer brushes. Chapter 4 reports our study on the conformational aspects and intramolecular phase separation of alternating copolymacromonomers using the BFM. The architecture which is being investigated consists of a comb copolymer brush with two different types of side chains alternatingly grafted along the backbone. By evaluating angular correlation histograms we examine the phase separation of the side chains with increasing chemical incompatibility. Provided the backbone is stiff, we observe a pearl necklace-like transition in poor solvent. When the backbone is flexible it is possible to obtain meandering and horseshoe like conformations by imposing different solvent conditions on both side chain types.

Chapter 5 reports our simulation study discussing spontaneous curvature of comb copolymers strongly adsorbed at a flat surface. The simulations in this study are athermal and concern densely grafted 2D comb copolymers. Two different cases are investigated, the difference being whether the side chains are allowed to flip from one side of the backbone to the other side. When the side chains are allowed to flip the polymers display a distinct curvature. This is illustrated using bond angle correlation plots as well as scattering analysis. A theoretical model, including both curvature and stiffness, is outlined that is able to fit the data. The main findings are in agreement with recent theoretical and experimental studies.

Chapter 6 discusses our simulation study on cylindrical core-shell structures formed by dendrite-like polymers in selective solvent. Using dendronized side chains rather than linear side chains a core-shell structure is formed in selective solvent. Three cases are being distinguished: the athermal case in which the conformational properties are governed by excluded volume only, the case in which the shell experiences good solvent whereas the core experiences moderate solvent and the case in which the core experiences poor solvent. It is demonstrated, using bond angle correlation plots as well as scattering data, that the poor solvent case exhibits significantly different behavior from both other cases. The poor solvent case displays curvature whereas the other two show simple persistent wormlike chain behavior. Our theoretical model, discussed in Chapter 5 was found to be able to fit the data quite well. If persistence and curvature could be increased it may be possible to obtain ring closure depending on solvent conditions or temperature.

Chapter 7 discusses our simulation results on 2D comb copolymer brushes with a lower grafting density than those in Chapter 5. In that previous work it was suggested that the fact that spontaneous curvature did not turn up in other simulation studies is connected to the lower grafting density that was used there. Using the same model and conditions the grafting density has been decreased by a factor of three in Chapter 7. It is shown that spontaneous curvature is indeed lost and that the conformational properties of the comb copolymer are perfectly described as being persistent comb copolymer chain behavior. Our findings support the idea that a cross-over regime exists between lower grafting densities for which scaling analysis is valid and higher grafting densities for which scaling arguments are not acceptable anymore and mean field calculations have to be employed.

Part I

Introduction

1

Experimental Aspects of Cylindrical Polymer Brushes

Synthesis and molecular architecture of cylindrical polymer brushes

Molecular bottlebrushes

Since the first successful polymerisation of macromonomers by Tsukahara and coworkers [1–4], a large body of experimental work has been published on the investigation of comb copolymers with long side chains and a high grafting density. Besides the polymerisation of macromonomers alternative routes have recently been developed using grafting from a macroinitiator prepared by either atom-transfer radical polymerisation [5] or by living cationic polymerisation [6].

The first molecular brushes were synthesised using the macromonomer approach, for which anionically prepared oligostyrenes with metacryloyl end-groups were homopolymerised using the radical polymerisation mechanism. The molecular brush thus obtained is illustrated in the cartoon of Figure 1.1. Since this thesis is devoted to computer simulations of molecular brushes a typical snapshot, i.e. a graphical representation of the state of the polymer brush in computer memory at a certain point during a simulation, is shown in Figure 1.2.

The addition of side chains leads to increased stiffness causing molecular brushes in solution to be stretched more when compared to their linear counterparts or even to assume a (wormlike) cylindrical shape. It is commonly accepted that this increase in stretching and stiffness is due to steric repulsion between the side chains. Further on in this chapter some of the theoretical work as well as simulations on this subject will be discussed.

Dendronized polymers

A variation on the concept of the molecular brush are dendronised polymers. Instead of having linear side chains dendrons are grafted to the backbone, i.e. the side chain material exhibits branching points at which the chain splits up into several others. Multiple generations of branching are conceivable. These type of molecules have been discussed in a recent review by Schlüter and Rabe [7]. The dendritic nature of the side chain material causes the monomer density to drop much slower when going from the interior to the exterior than is the case for the molecular brush.

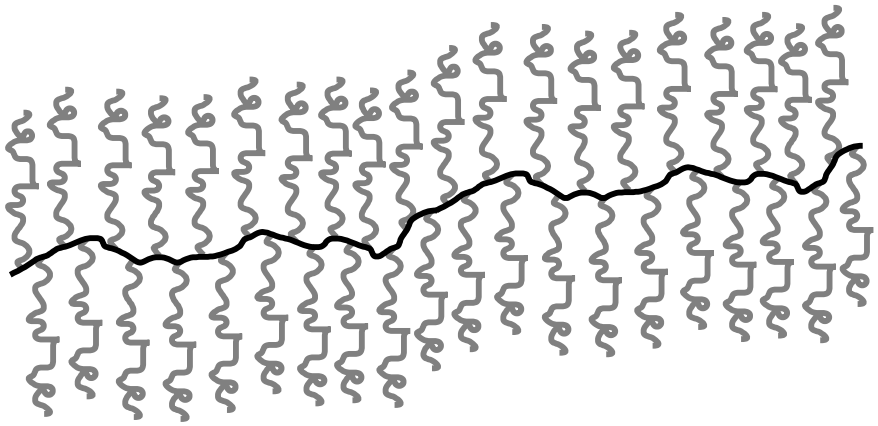

Figure 1.1: Schematic representation of a molecular bottlebrush.

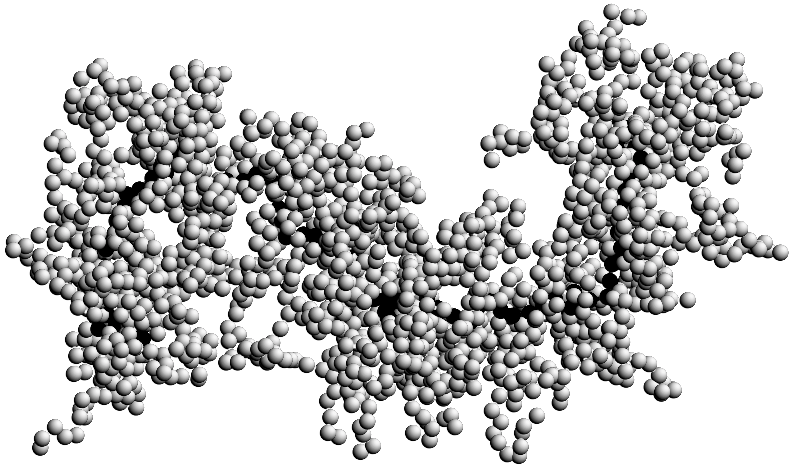

Figure 1.2: Typical computer simulation snapshot of a molecular bottlebrush in a dilute solution with good solvent. The backbone (black) consists of 100 segments. The number of side chains (grey) equals 100, each consisting of 10 segments.

Due to the increased steric repulsion cylindrical structures that are even stiffer than molecular brushes will be obtained in solution. Figures 1.3 and 1.4 illustrate the architecture of an dendronised polymer and a typical snapshot in a dilute solution with good solvent respectively. In chapter 6 a computer simulation study will be presented involving dendritic-like side chains.

Heterografted copolymer brushes

Being a specific subclass of molecular bottlebrushes heterografted copolymer brushes feature two chemically different kinds of polymeric side chains that are statistically or alternatingly distributed along the backbone. Schmidt and coworkers [8] have prepared heterografted brush molecules consisting of poly(2-vinyl pyridine) (P2VP) and poly(methyl metacrylate) side chains via the macromonomer approach. An illustration of this type of system is shown in Figure 1.5.

Typical wormlike cylinders have been observed by atomic force microscopy (AFM) for the copolymers spin-cast, i.e. a small amount of polymer solution evenly distributed on a rotating substrate, from chloroform onto mica. After quaternisation, i.e. the process of positively charging by adding protons, of the P2VP side chains the chemical incompatibility between the different types of side chains was increased causing intramolecular phase separation that remained intact during the drying process. When the polymers were spin-cast from a selective solvent, i.e. when the solvent quality for both side chain types is distinctively different, curved structures were observed by AFM. Among these structures were typical horseshoe brushes and meandering brushes. Figure 1.6 illustrates the postulated intramolecular phase separation and the effect of the selective solvent.

A most recent example of heterografted brush copolymers involved side chains of poly(ethylene oxide) and poly(*n*-butylacrylate) [9]. No information was given about intramolecular phase separation.

If the presence of two chemically different side chains leads to intramolecular phase separation so-called molecular Janus cylinders are formed. These are part of a larger class of Janus micelle nanoparticles described in some detail in a recent review paper by Mori and Müller [10]. Janus micelles are characterised by a compartimentalisation of the different ‘grafts’ involved. The phrase ‘Janus’ refers to the property of having two faces.

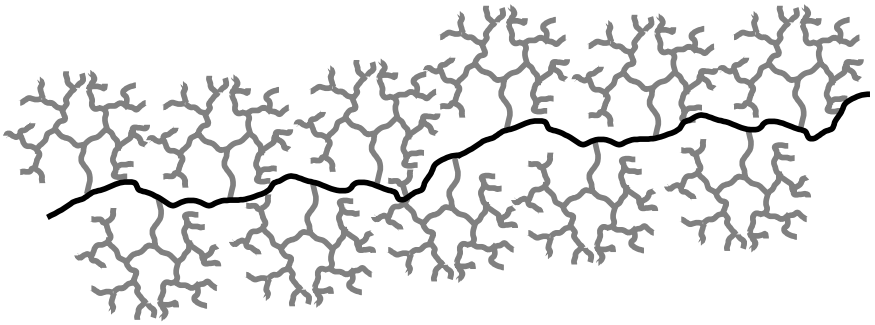

Figure 1.3: Schematic representation of a dendronized polymer.

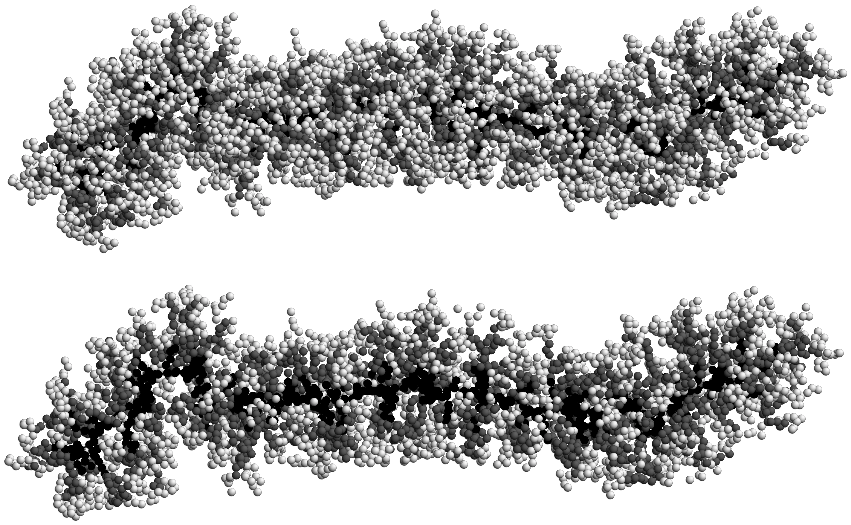

Figure 1.4: Typical computer simulation snapshot of a dendronised polymer in a dilute solution with good solvent. The backbone consists of 100 segments. The number of side groups equals 100, each branching into two chains after 5 segments for 3 generations (i.e. 75 segments per side group). The lower picture shows a cross section. Lighter grey values indicate higher level branchings.

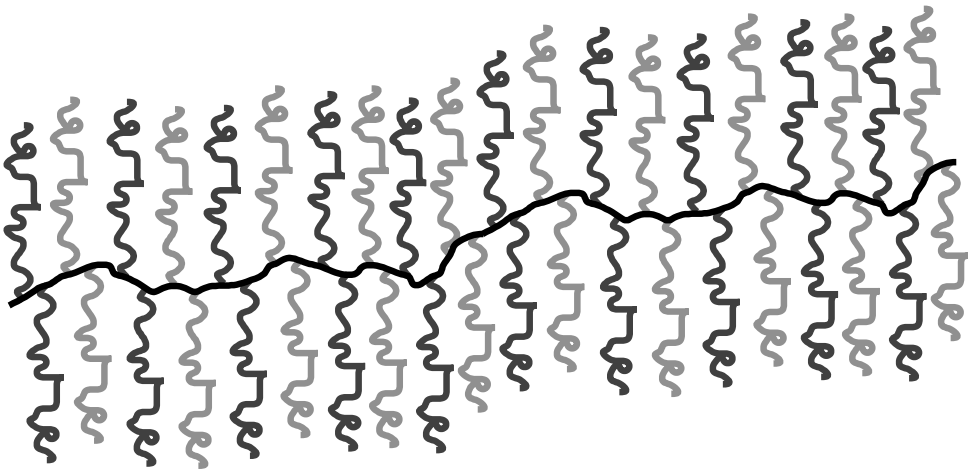

Figure 1.5: Illustration of a heterografted brush with alternatingly different side chains.

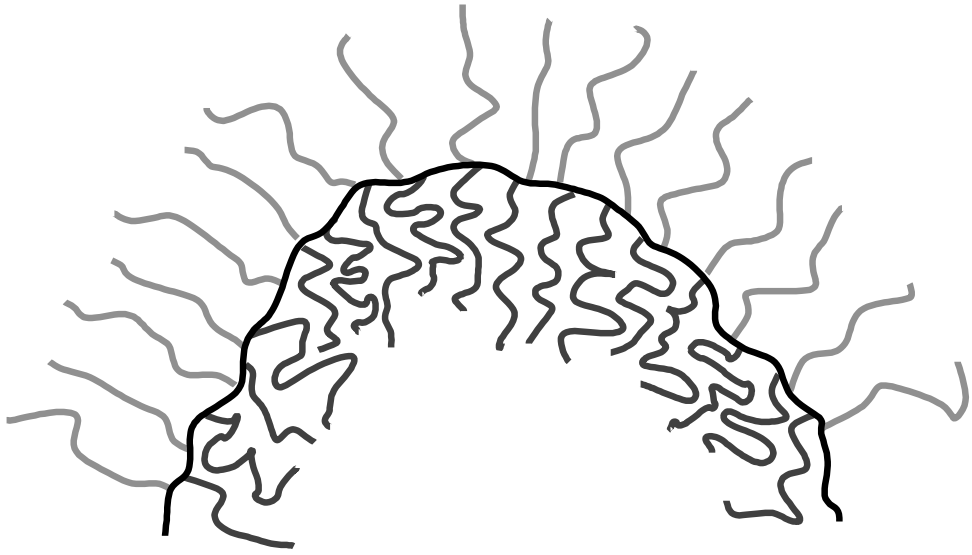

Figure 1.6: Illustration of postulated intramolecular phase seperation. The side chains have phase seperated. Since the solvent is worse for the bottom part the side chains assume a more compact arangement there. This results in bending.

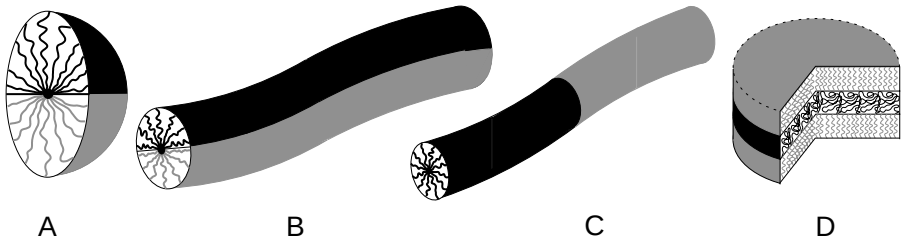

Figure 1.7: A number of possible Janus micelles: (A): Janus sphere. (B) and (C): Janus cylinders. (D): Janus sheet.

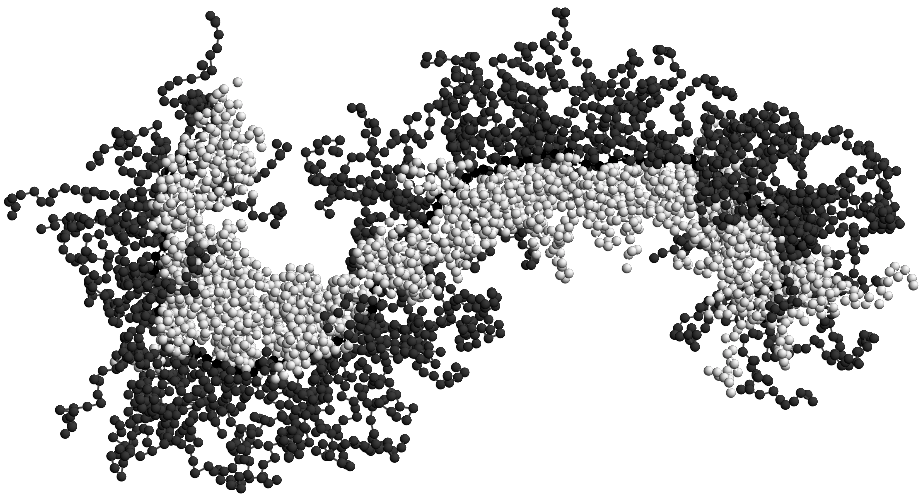

Figure 1.8: Snapshot from our computer simulation study of heterografted molecular brushes. White side chains experience θ solvent and dark grey side chains good solvent conditions.

A simple classification of the different Janus micelles, as given in ref. [10] is presented in Figure 1.7, however far more complex micellar structures may be envisioned as well.

Several examples of intramolecular phase separation observed from computer simulations are described in Chapter 4 [11]. A snapshot of a Janus-like structure obtained by intramolecular phase separation is shown in Figure 1.8. A complete discussion will be given in Chapter 4.

Brush-block-brush copolymers

A straightforward extension of the heterografted brushes is the class of brush-block-brush copolymers. In this case the two chemically different types of side chains are, rather than statistically or alternatingly, sequentially attached to the backbone leading to a block type double brush. Figure 1.9 illustrates this type of copolymer brush. Sogabe and coworkers [12] have synthesised brush-block-brush copolymers involving poly(ethylene glycol methylether) (PEG) side chains as well as poly(2-hydroxyethyl methacrylate) (PHEMA) side chains using atom transfer radical polymerisation. Due to the relatively short backbone (70 units versus 45 (PEG) and 21 (PHEMA)) the brushes exhibited a spherical or ellipsoidal shape rather than a cylindrical shape.

Figure 1.10 shows a snapshot from a computer simulation study of a brush-block-brush type copolymer. The main chain consists of 100 segments and there are 100+100 side chains of 20 segments each. Note that the dark part of the molecule is more compressed due to different solvent conditions.

Molecular brushes with block copolymer side chains

In recent years the interest in nanoscience has assumed enormous proportions. The formation of e.g. nanowires or ordered arrays of metal and semiconductor clusters is a hot item. A possible approach to obtain these kind of nanostructures is by utilising amphipolar core-shell cylindrical brushes as templates. For example metal ions from solution may be deposited into the polar core providing a conducting wire isolated by the non-polar outer blocks after evaporating the solvent.

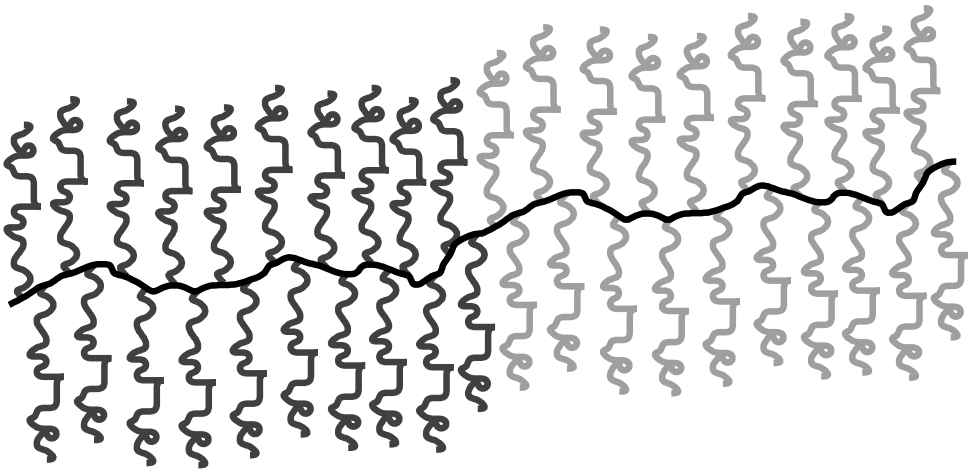

Figure 1.9: Illustration of a brush-block-brush.

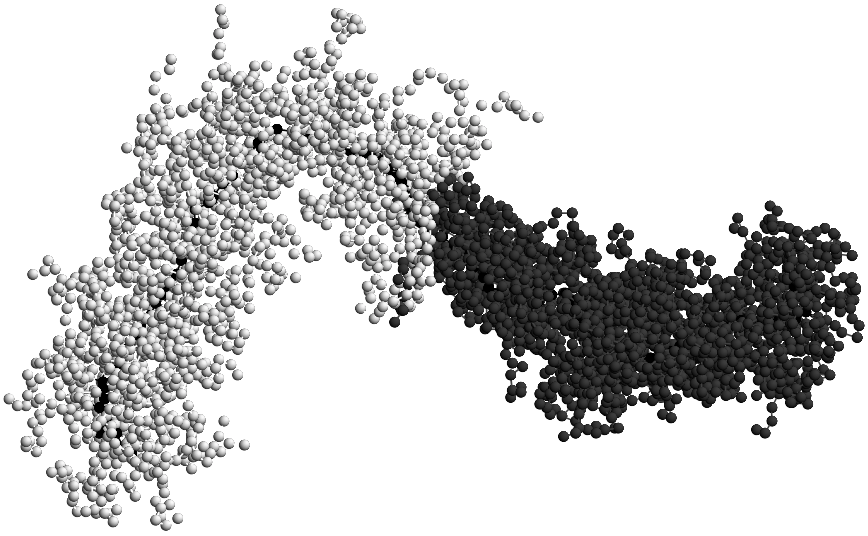

Figure 1.10: Snaphot from a computer simulation for a brush-block-brush copolymer molecule. Dark grey side chains experience θ-solvent and white side chains good solvent conditions. This is an example of Janus micelle C as depicted in Figure 1.7.

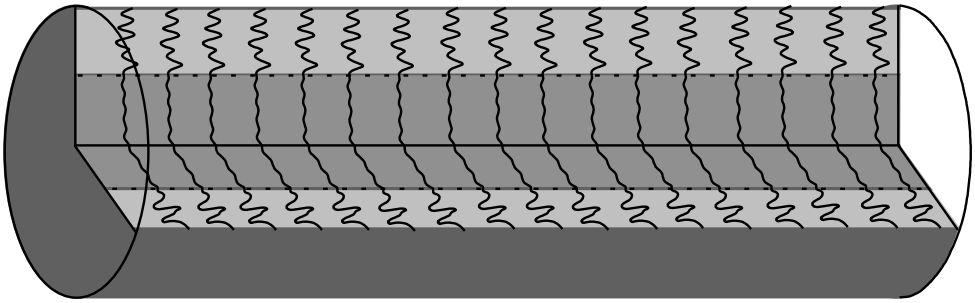

Figure 1.11: Illustration of a brush with diblock side chains.

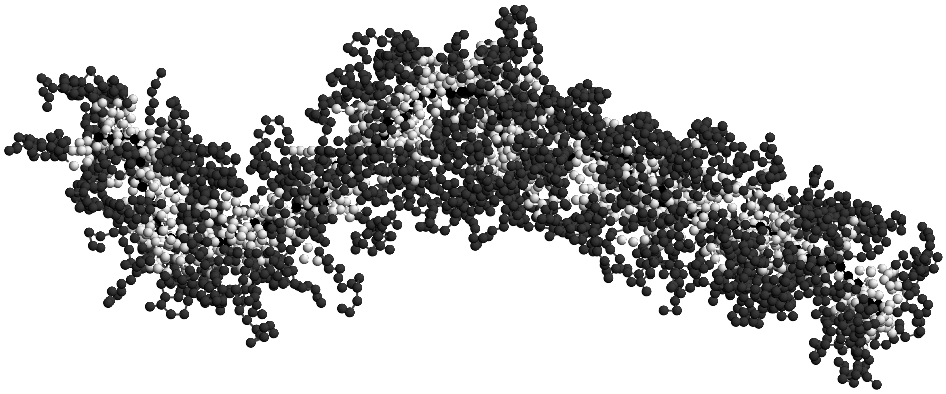

Figure 1.12: Snaphot from a computer simulation for a brush copolymer molecule with diblock side chains. White side chains (core) experience good solvent and dark grey side chains (shell) θ solvent conditions.

A straightforward way to prepare amphipolar core-shell cylindrical brushes is by employing amphiphilic diblock copolymer side chains. Using a suitable selective solvent intramolecular phase separation will occur, leading to a core-shell morphology as illustrated in Figure 1.11. An example of intramolecular phase separation occurring in these kind of copolymer brushes as obtained by computer simulation is given in Figure 1.12. The synthesis of core-shell molecular brushes has been discussed in several papers [13–17].

Star molecular brushes

Instead of a single backbone with side groups it is of course possible to create more complex architectures incorporating the brush concept. Among these possibilities are the star-like brushes involving three or more brush arms emerging from a common centre. The synthesis of this class of copolymers is discussed in e.g. refs. [18, 19]. Figure 1.13 illustrates the architecture of a star molecular brush, while Figure 1.14 shows a typical snapshot from a 2D simulation of a three arm star, corresponding to e.g. the case of a star molecular brush adsorbed to a surface.

Dilute solution properties of cylindrical polymer brushes

The experimental characterisation of the comb copolymer brush conformation in dilute solution turned out to be a nontrivial issue. It was achieved recently by Schmidt and coworkers [20–27] using a combination of light scattering experiments and theoretical modelling. Since the high grafting density leads to a stiff molecular structure, the modelling has been based on the Kratky-Porod worm-like chain model. This model involves the Kuhn statistical segment length $l_K = 2\lambda$, where λ is the persistence length, and the contour length L as essential parameters. Expressions for the radius of gyration and the hydrodynamic radius in terms of λ and L can be found in the literature [28–31]. The expression for the radius of gyration in the Kratky-Porod model takes the form

$$R_g^2 = \frac{Ll_K}{6} - \frac{l_K^2}{4} + \frac{l_K^3}{4L} - \frac{l_K^4}{8L^2}\left(1 - \exp\left(-2L/l_K\right)\right) \qquad (1.1)$$

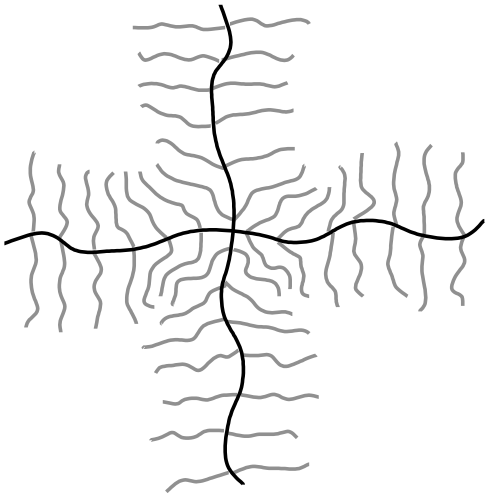

Figure 1.13: Illustration of a 4 arm star molecular brush.

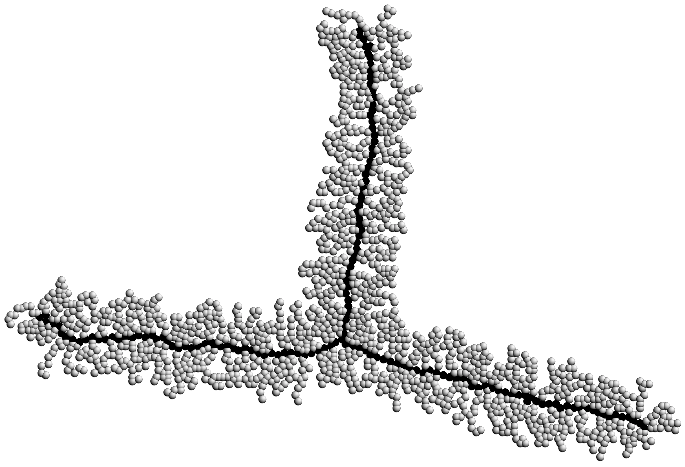

Figure 1.14: Snapshot from a 2D computer simulation of a 3 arm star molecular brush. The arms contain 50 segments and carry 50 side chains of length 10.

The analysis of the experimental light scattering data of various comb copolymer cylindrical brushes was originally based on this model. Here the contour length L of the worm-like cylinder is a parameter of crucial importance. By assuming that the contour length per monomer l is equal tot the maximum all-trans value of 0.25*nm*, it follows in a straightforward way from the degree of polymerisation P ($L = Pl$). Subsequently, the determination of the radius of gyration by light scattering allows for the evaluation of the Kuhn statistical segment length, and therefore the persistence length, using equation 1.1.

However, the approximation for the contour length per monomer to be equal to the all-trans value is clearly at variance with the computer simulation results to be discussed further on, which demonstrate a locally strongly fluctuating backbone. In addition, scanning force microscopy (SFM) and light scattering data can only be reconciled if l is assumed to be much smaller than the maximum all-trans value. As will be discussed in more detail in the next section, scanning force microscopy shows the dry two-dimensional state when the solvent has been evaporated. The contour length determined from SFM pictures possibly differs considerably from the values in dilute solution for which the scattering data are obtained.

However, Schmidt and coworkers [25–27] subsequently demonstrated a method to determine the length l per vinylic main chain monomer from the experimentally accessible form factor $S(q)$ as obtained from scattering experiments. For intermediate values of q the form factor behaves as $S(q) \propto q^{-1/\nu}$, where ν is the scaling exponent. For smaller length scales, i.e. larger values of q, the cylindrical brush will behave like a rigid rod and in particular $S(q) \propto q^{-1}$ for length scales smaller than the Kuhn statistical segment size. In the so-called Holtzer form $qS(q)$ is plotted against q. In such a Holtzer plot a horizontal plateau is reached for $ql_K \gg 1$. The height of this Holtzer plateau equals πM_L, where M_L is the mass per unit length of the worm-like cylinder and therefore inversely proportional to l

$$\lim_{ql_K \gg 1} qS(q) = \pi M_L \tag{1.2}$$

Figure 1.15 shows the backbone conformation from the snapshot of the comb copolymer brush discussed in section 1, page 4 (Figure 1.2). Despite the cylindrical shape with a persistence length $\lambda = 23$ segments, locally

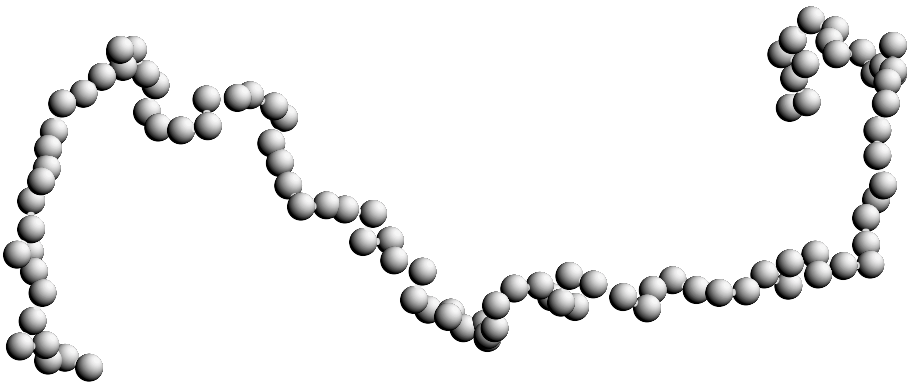

Figure 1.15: The backbone conformation of the bottlebrush from Figure 1.2. Despite the elongated shape, due to the presence of side chains, the backbone locally appears quite flexible.

the backbone appears very flexible. Clearly, it is far from being completely stretched. The persistence length was found from a bond angle correlation plot, a method that will be discussed in more detail in chapter 5.

Figure 1.16 shows a number of Holtzer plots for comb copolymer brushes in good solvent obtained from computer simulation where only the backbone segments acted as scatterers. The most flexible of these ($N = 10, \sigma = 1$) does not reach a horizontal plateau. However, the $N = 20$, $\sigma = 1$ system does reach a plateau with $qS(q) \approx 1.5$, corresponding to a contour length per segment of $l \approx 2.1$. This should be compared to the distance between segments which, in the bond fluctuation model employed, is allowed to vary between 2 and $\sqrt{10}$. In fact, the calculated mean distance per segment in this case is $\langle b \rangle \approx 2.81$, which is significantly larger than l. This confirms the statement about the local flexibility of the backbone leading to a far from stretched backbone conformation.

Clearly, the $N = 20$, $\sigma = 2$ system reaches a horizontal plateau for much smaller values of q, which is consistent with a larger Kuhn statistical segment size. In addition, the height of the plateau ($qS(q) \approx 1.2$) is significantly lower, corresponding to a contour length per segment of $l \approx 2.6$ while the

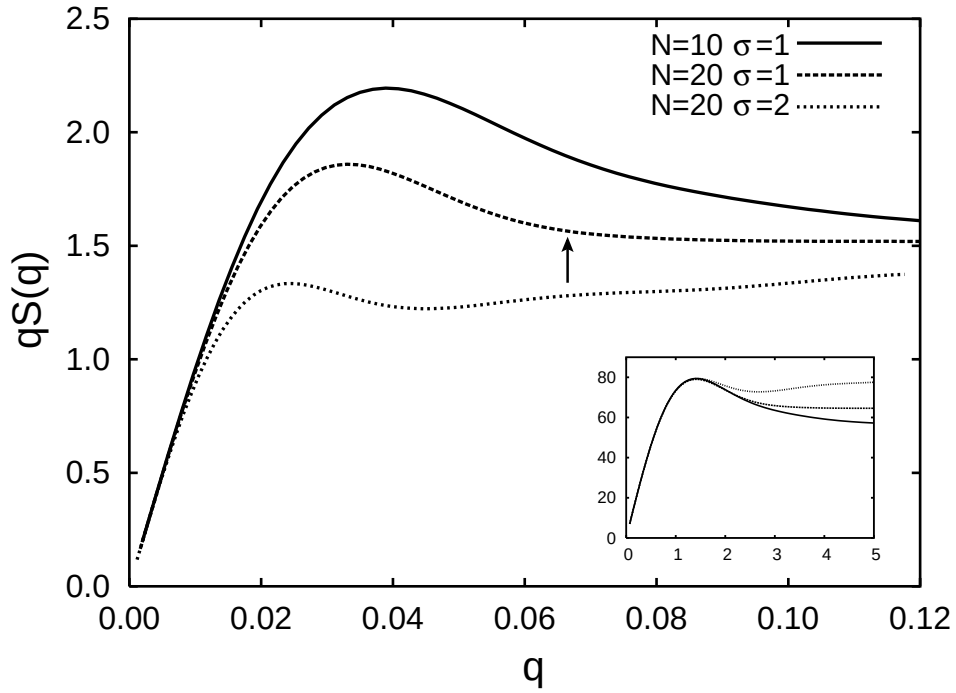

Figure 1.16: Holtzer plot of several bottlebrush polymers in good solvent. The backbone length is 100 segments, the side chain lengths 10 and 20 segments, and the grafting density 1 and 2. The arrow indicates the value of q corresponding to the Kuhn statistical segment length for the $N = 20$, $\sigma = 1$ system. Inset: the same plots with both axes multiplied by R_g. Note that the tops have merged.

mean distance per segment now equals $\langle b \rangle \approx 2.96$. Doubling the amount of side chains has increased the stretching of the backbone, however, it is still not fully stretched.

The arrow in Figure 1.16 denotes the value of q corresponding to the Kuhn statistical segment length l_K for the $N = 20$, $\sigma = 1$ system. This value was obtained from $l_K \approx 2\lambda = 46$ segments and by making use of the contour length per segment, giving $l_K \approx 95$. The Kuhn statistical segment length can also be obtained from equation 1.1 and the Holtzer plot. Dividing eqn. 1.1 by L^2, the right hand side can simply be written in terms of l_k/L. The radius

of gyration is obtained from the Holzer plot by making use of the property that for the position of the maximum $\langle R_g^2 \rangle^{1/2} q = 1.4$ for wormlike chains, yielding $\langle R_g^2 \rangle^{1/2} = 42.4$. This agrees excellently with the value $\langle R_g^2 \rangle^{1/2} = 42.5$ obtained from

$$R_g^2 = \frac{1}{2N^2} \sum_{k=0}^{N-1} \sum_{l=0}^{N-1} (\vec{r}_k - \vec{r}_l)^2 \tag{1.3}$$

The contour length is simply the product of the number of backbone segments and the contour length per segment giving $L = 207$. Using the modified version of eqn. 1.1 it is found that $l_k/L \approx 0.452$, corresponding to $l_k \approx 93.6$ and in very good agreement with the previous value.

The inset of Figure 1.16 shows the same plots but with both axes multiplied with R_g. Holtzer plots are commonly presented in this form in computer simulation studies as the positions of the tops of the plots merge for systems with the same number of scatterers. In experimental studies it is more common to normalise the y-axis with respect to the height of the Holtzer plateau as this makes it possible to immediately read of the ratio of the height of the top to that of the plateau. This ratio is proportional to the number of Kuhn segments in the polymer chain.

An alternative way of finding the Kuhn statistical segment length from scattering data is by making use of a so-called Kratky plot in which $q^2 S(q)$ is plotted versus q. In such a Kratky plot a plateau is reached for the Gaussian scaling regime, while the persistent regime shows up as a straight line with slope 1. From the intersection of both asymptotes the Kuhn statistical segment length can be found as $l_K = 12/(\pi q_{int})$. The downside of this method is that the Gaussian scaling plateau diminishes when less Kuhn segments are present and disappears completely when the number drops below 4. This is illustrated for the $N = 20$, $\sigma = 1$ system in Figure 1.17.

Experimentally, for high molar mass polymacromonomers based on methacryloyl end-functionalised oligo mathacrylates ($M_n = 2410$ g/mol) in the good solvent THF, the length l per vinylic main chain monomer was found to be a mere 0.071 nm per monomer, significantly lower than the 0.25 nm all-trans value [27]. The Kuhn statistical segment length $l_K = 2\lambda$ turned out to be 120 nm.

For polymacromonomers ($M_n = 3624$ g/mol) consisting of polystyrene main and side chains these values are $l = 0.145$ nm, $l_K = 190$ nm in the good

solvent toluene and l = 0.11 nm, l_K = 120 nm in the 'θ-solvent' cyclohexane. These results compare favourably with the computer simulation results. In particular the fact that the length of the worm-like cylinder per vinylic main chain monomer is considerably smaller than the all-trans value is qualitatively in excellent agreement with the simulation data.

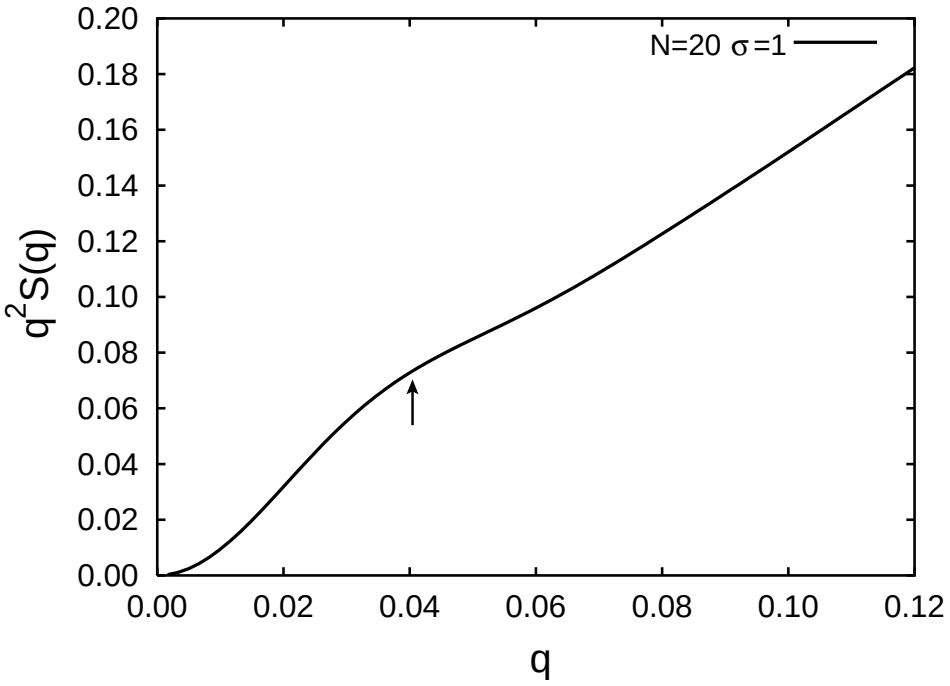

Figure 1.17: Kratky plot of the N = 20, σ = 1 system. The arrow indicates the value of q for which a kink should be present.

AFM of cylindrical polymer brushes

Atomic force microscopy has been used extensively to visualise molecular brush conformations [23, 24, 32, 33]. In many cases the stiff cylinder-like structure was confirmed. However, care should be taken when directly comparing the 2D images with the 3D dilute solution situation since 2D confinement may lead to significant additional stretching. Still, these studies convincingly demonstrated that even under 2D confinement the polymer backbones of the molecular brushes are far from being fully extended.

A most striking observation concerns the presence of spiralling conformations for molecular brushes strongly adsorbed onto a flat substrate [34, 35]. In a first explanation of the unexpected spiral-like conformations an unequal distribution of side chains to both sides of the backbone was postulated [36]. Such an uneven distribution may simply arise due to the strong adsorption of the side chains to the substrate thus leading to a quenched uneven distribution. Figure 1.18 shows a snapshot from our computer simulations featuring a similar conformation obtained by a 2D simulation of a molecular brush with an uneven distribution of side chains imposed.

In a further study of this phenomenon, the authors concluded that in fact spontaneous curvature occurred for molecular brushes adsorbed on a flat substrate [35, 37]. Under conditions in which flipping of the side chains from one side to the other is possible an uneven distribution of side chains is thermodynamically favourable and therefore resulting in bending of the molecular brush. Equilibration was achieved experimentally using alternately compression and expansion of a brush monolayer followed by its transfer onto a mica substrate. A theoretical analysis confirmed the 2D spontaneous curvature. We have addressed this issue by computer simulations that will be discussed in detail in Chapter 5.

Applications of cylindrical polymer brushes

Although several applications of shape persistent objects such as molecular brushes may be envisioned, two different types of applications have actually been discussed in the literature so far. The first one uses the induced collapse from cylindrical brushes to spheres either for the design

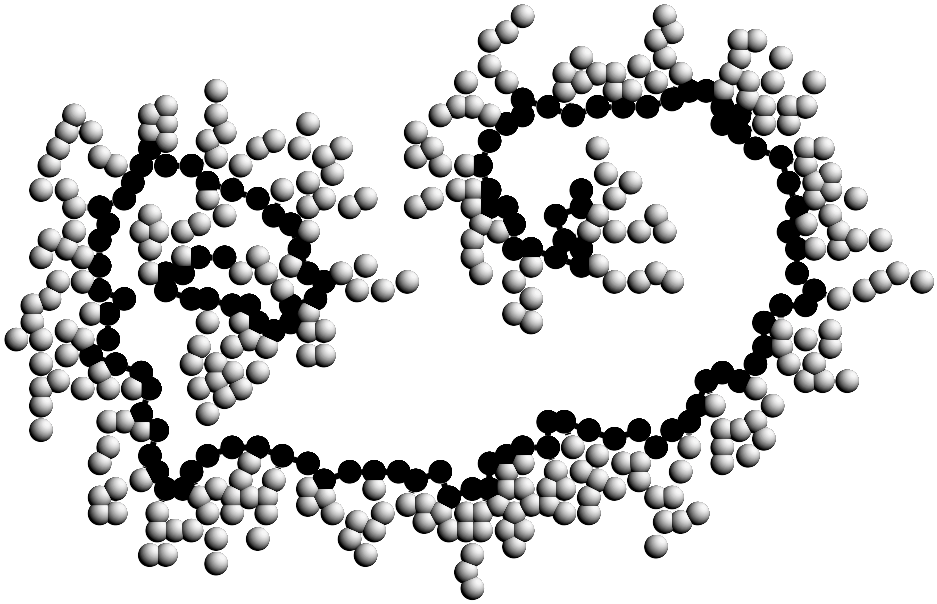

Figure 1.18: 2D computer simulation snapshot of a comb copolymer with a backbone of 120 segments and 60 side chains of length 5. The side chains are all placed on the same side of the backbone causing it to bend.

of a molecular actuator or as a kind of 'valve' in the design of environment-responsive nanoporous systems. The latter has not yet been developed beyond the drawing board stage [38]. The thermally induced collapse of single macromolecules from cylindrical brushes to spheres has been achieved using molecular brushes with poly-*N*-isopropyl-acrylamide (PNIPAM) side chains [39]. PNIPAM is well known for its lower critical solution temperature (LCST) behavior in aqueous solution [40] and a temperature jump induces the collapse.

Furthermore, the conformational switching of molecular brushes in response to the energy of interaction with a substrate has been realised experimentally as well [41–43]. The Langmuir-Blodgett technique was used to compress monolayers of molecular brushes with poly(*n*-butyl acrylate) side chains. The energy of interaction with the substrate was varied by changing

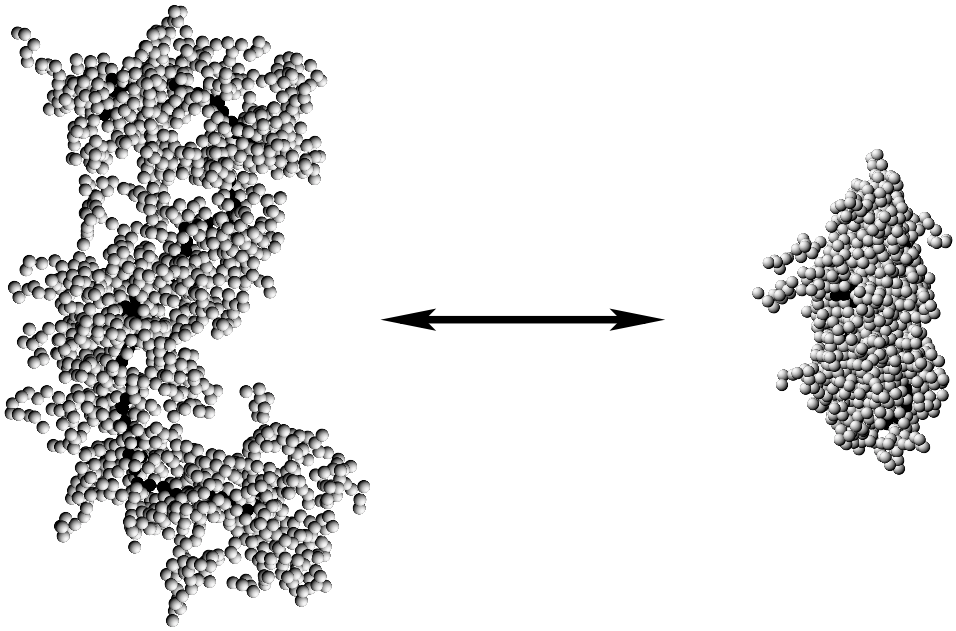

Figure 1.19: 3D computer simulation snapshots of the same bottlebrush molecule in good and poor solvent. The system is identical to that in Figure 1.2.

the substrate composition by mixing water (higher surface energy) with methanol (lower surface energy). The conformational changes observed result from the partial desorption of the side chains when the surface energy is reduced [42]. In a most recent example conformational transitions were observed for poly(methacrylate)-*g*-poly(*n*-butylacrylate) brush-like macromolecules spin-cast on mica and then exposed to a mixed water/ethanol vapour [43]. Figure 1.19 illustrates a typical 3D brush-globule transition taken from a computer simulation.

The second class of applications explores the amphipolar character of core-shell cylindrical brushes. Encapsulation of conducting polymers was achieved by the oxidation polymerisation of pyrrole inside the poly(2-vinyl pyridine) core of a copolymer brush obtained by radical polymerisa-

tion of vinylbenzyl-terminated poly(α-methylstyrene)-*b*-poly(2-vinyl pyridine) macromonomers. Cu^{2+} ions (oxidant) were introduced in the P2VP domains [44]. In another example methacryloyl end-functionalised polystyrene-*b*-poly(2-vinyl pyridine) macromonomers were used to prepare amphipolar core-shell cylindrical brushes. The P2VP core was loaded with $HAuCl_4$ in toluene or methylene chloride followed by reduction. Depending on the amount of noble metal ions and the reduction conditions, either a linear metal cluster array or a continuous nanowire was formed [45].

Recently, along the same line, superparamagnetic hybrid nanocylinders were produced by Müller and co-workers [46–48]. Core-shell cylindrical brushes were prepared from brushes with poly(acrylic acid)-*b*-poly(*n*-butyl acrylate) side chains. The carboxylic acid groups of the poly(acrylic acid) core can coordinate with various metal ions such as Fe^{3+} and Fe^{2+} The authors performed an alkaline oxidation of ferrous ions to fabricate magnetic nanoparticles. The hybrid nanocylinders were found to be superparamagnetic at room temperature.

References

[1] Y. Tsukahara, K. Mizuno, A. Segawa, Y. Yamashita, *Macromolecules* **1989**, *22*, 1546.

[2] Y. Tsukahara, K. Tsutsumi, Y. Yamashita, *Macromolecules* **1989**, *22*, 2869.

[3] Y. Tsukahara, K. Tsutsumi, Y. Yamashita, S. Shimada, *Macromolecules* **1990**, *23*, 5201.

[4] Y. Tsukahara, in: *Macromolecular design: concept and practice*, M. Misra, ed., Polymer Frontiers International Inc., New York 1993, pp. 161–227.

[5] K. Beers, G. Scott, K. Mattyjaszewski, S. Sheiko, M. Möller, *Macromolecules* **1998**, *31*, 9413.

[6] M. Schappacher, C. Billaud, C. Paulo, A. Deffieux, *Macromol. Chem. Phys.* **1999**, *200*, 2377.

[7] A. D. Schlüter, J. P. Rabe, *Angew. Chem. Int. Ed.* **2000**, *39*, 864.

[8] T. Stephan, S. Muth, M. Schmidt, *Macromolecules* **2002**, *35*, 9857.

[9] D. Neugebauer, Y. Zhang, T. Pakula, K. Matyjaszewski, *Polymer* **2003**, *44*, 6863.

[10] H. Mori, A. Müller, *Prog. Poly. Sci* **2003**, *28*, 1403.

[11] J. de Jong, G. ten Brinke, *Macromol. Theory Simul.* **2004**, *13*, 318.

[12] K. Ishizu, J. Satoh, A. Sogabe, *J. Colloid Interface Sci.* **2004**, *274*, 472.

[13] R. Djalali, N. Hugenberg, K. Fischer, M. Schmidt, *Macromol. Rapid. Commun.* **1999**, *20*, 444.

[14] K. Tsubaki, K. Ishizu, *Polymer* **2001**, *42*, 8387.

[15] H. Börner, K. Beers, K. Matyjaszewski, S. Sheiko, M. Möller, *Macromolecules* **2001**, *34*, 4375.

[16] G. Cheng, A. Böker, M. Zhang, G. Krausch, A. Müller, *Macromolecules* **2001**, *34*, 6883.

[17] M. Zhang, T. Breiner, H. Mori, A. H. E. Müller, *Polymer* **2003**, *44*, 1449.

[18] K. Matyjaszewski, S. Qin, J. R. Boyce, D. Shirvanyants, S. S. Sheiko, *Macromolecules* **2003**, *36*, 1843.

[19] N. Hadjichristidis, M. Pitsikalis, H. Iatrou, S. Pispas, *Macromol. Rapid. Commun.* **2003**, *24*, 979.

[20] M. Wintermantel, M. Schmidt, Y. Tsukahara, K. Kajiwara, S. Kohjiya, *Macromol. Rapid. Commun.* **1994**, *15*, 279.

[21] M. Wintermantel, K. Fischer, M. Gerle, R. Ries, M. Schmidt, K. Kajiwara, H. Urakawa, I. Wataoka, *Angew. Chem. Int. Ed. Engl.* **1995**, *34*, 1472.

[22] M. Wintermantel, M. Gerle, K. Fischer, M. Schmidt, I. Wataoka, H. Urakawa, K. Kajiwara, Y. Tsukahara, *Macromolecules* **1996**, *29*, 978.

[23] P. Dziezok, S. Sheiko, K. Fischer, M. Schmidt, M. Möller, *Angew. Chem. Int. Ed. Engl.* **1997**, *36*, 2812.

[24] S. Sheiko, M. Gerle, K. Fischer, M. Schmidt, M. Möller, *Langmuir* **1997**, *13*, 5368.

[25] M. Gerle, K. Fischer, S. Roos, A. Müller, M. Schmidt, S. Sheiko, S. Prokhorova, M. Möller, *Macromolecules* **1999**, *32*, 2629.

[26] K. Fischer, M. Gerle, M. Schmidt, *Proc ACS PMSE Anaheim* **1999**, *30*, 133.

[27] K. Fischer, M. Schmidt, *Macromol. Rapid. Commun.* **2001**, *22*, 787.

[28] Yamakawa, "*Modern theory of polymer solutions*", Harper and Row, New York 1971.

[29] M. Schmidt, W. H. Stockmayer, *Macromolecules* **1984**, *17*, 509.

[30] R. C. Oberthür, *Makromol. Chem.* **1978**, *179*, 2693.

[31] R. Koyama, *J. Phys. Soc. Jap.* **1973**, *34*, 1029.

[32] S. Sheiko, *Adv. Polym. Sci.* **2000**, *151*, 61.

[33] S. Sheiko, M. Möller, *Chem. Rev.* **2001**, *101*, 4099.

[34] P. G. Khalatur, A. R. Khokhlov, S. A. Prokhorova, S. S. Sheiko, M. Möller, P. Reineker, D. G. Shirvanyanz, N. Starovoitova, *Eur. Phys. J. E* **2000**, *1*, 99.

[35] I. Potemkin, A. Khokhlov, S. Prokhorova, S. Sheiko, M. Möller, K. Beers, K. Matyjaszewski, *Macromolecules* **2004**, *37*, 3918.

[36] I. Potemkin, A. Khokhlov, P. Reineker, *Eur. Phys. J. E* **2001**, *4*, 93.

[37] I. Potemkin, *Eur. Phys. J. E* **2003**, *12*, 207.

[38] S. P. Adiga, D. W. Brenner, *Nano Lett.* **2002**, *2*, 567.

[39] C. Li, N. Gunari, K. Fischer, A. Janshoff, M. Schmidt, *Angew. Chem. Int. Ed.* **2004**, *43*, 1101.

[40] C. Wu, S. Zhou, *Phys. Rev. Lett.* **1996**, *77*, 3053.

[41] M. O. Gallyamov, B. Tartsch, A. R. Khokhlov, S. S. Sheiko, H. G. Börner, K. Matyjaszewski, M. M. Möller, *Macromol. Rapid. Commun.* **2004**, *25*, 1703.

[42] S. Sheiko, S. Prokhorova, K. Beers, K. Matyjaszewski, I. Potemkin, A. Khokhlov, M. Möller, *Macromolecules* **2001**, *34*, 8354.

[43] F. Sun, S. S. Sheiko, M. Möller, K. Beers, K. Matyjaszewski, *J. Phys. Chem. A* **2004**, *108*, 9682.

[44] K. Ishizu, S. Tsubaki, K. Uchida, *Macromolecules* **2003**, *35*, 10193.

[45] R. Djalali, S.-Y. Li, M. Schmidt, *Macromolecules* **2002**, *35*, 4282.

[46] M. Zhang, P. Teissier, M. Krekhova, V. Cabuil, A. H. E. Müller, *Progr. Colloid Polym. Sci.* **2004**, *126*, 35.

[47] C. P. León, L. Kador, M. Zhang, A. H. E. Müller, *J. Raman Spectrosc.* **2004**, *35*, 165.

[48] M. Zhang, C. Estournès, W. Bietsch, A. H. E. Müller, *Adv. Funct. Mater.* **2004**, *14*, 871.

2

Theoretical Aspects of Comb Copolymer Brushes

Ever since Zimm and Stockmayer [1] developed, in the late 40s, expressions that relate the size of branched molecules without excluded volume to the number and position of branches, there has been an interest in the conformational properties of these systems. Ptitsyn [2] and Kron and Ptitsyn [3] showed a decade later that the presence of branches increases the excluded volume effect which results in a swelling of the molecule. Their equations demonstrate that the expansion factor of branched macromolecules in good solvent is significantly larger than that of a linear polymer of the same length. The same conclusion was later made by Berry and Orofino [4]. It was only four decades later at about the same time that Tsukahara and coworkers were able to polymerize the first macromonomers that the theoretical investigation of individual comb copolymers really got started.

Individual comb copolymers in solution

The conformational characteristics of individual comb copolymers with a high grafting density of side chains in solution has been addressed in a series of theoretical papers [5–13] to begin with the original work of Birshtein and coworkers [5]. Irrespective of the solvent quality, be it a good solvent or a θ-solvent, all theories predict a cylindrical brush-like structure for sufficiently long side chains. The pertinent parameters are the side chain grafting density, σ, the side chain length M, the intrinsic stiffness of the backbone and the side chains and the solvent quality with respect to the side chains and the backbone. Essential quantities to characterize the conformations are the persistence length λ of the comb copolymer brush, the diameter D of the cylindrical structure and the *spatial* distance l between the grafting points (see Figure 2.1).

We will start with a scaling analysis of a comb copolymer brush that consists of a straight backbone to which flexible side chains of length M are attached. The grafting density will be denoted σ representing the number of side chains per length a. We will assume good, athermal, solvent conditions for the side chains and treat the backbone as a volumeless rigid rod of length $L = Na$. For a high grafting density, the interactions with the other chains forces a side chain away from the cylinder axis. The influence of the neighboring side chains can be described in terms of an effective field.

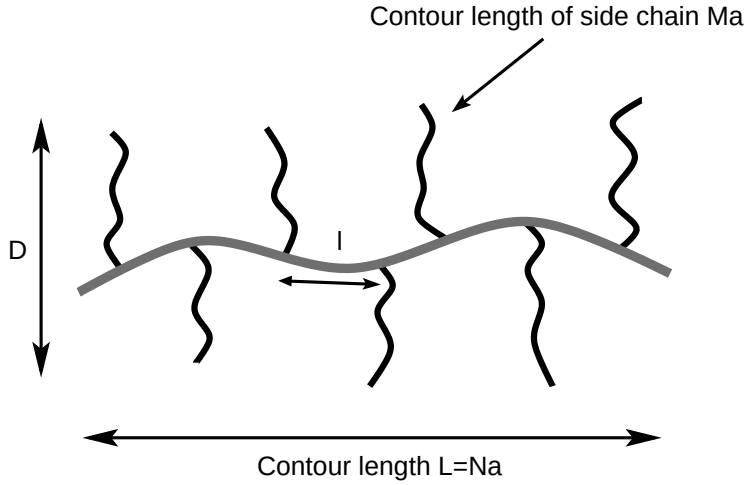

Figure 2.1: Cartoon of cylindrical comb copolymer brush illustrating the various parameters.

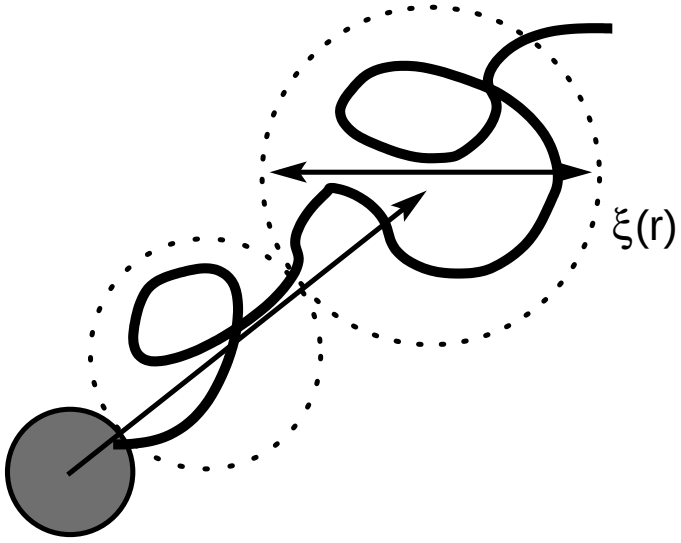

Figure 2.2: Illustration of the blob picture.

Near the cylinder axis the chains are stretched most and a side chain can be described as a series of blobs of increasing size [6, 14]. The size of a blob corresponds to the characteristic length of a small part of the side chain for which the trajectory is still determined by Brownian motion. Within a blob the trajectory is that of a Self-Avoiding Walk (SAW). Successive blobs, however, follow a outward directed trajectory. The kinetic energy responsible for the Brownian motion of the chain part in a blob is of the order kT. The characteristic size of a blob corresponds to an excess free energy due to the field of the neighboring side chains of the order of this kinetic energy kT. At a smaller length scale Brownian motion dominates, at a larger length scale the stretching field dominates. The total number of side chains equals $N\sigma$. The conformation of every side chain is a trajectory moving away from the cylinder axis. The side chain conformation consists of a succession of blobs of radius $\xi(r)$ (see Figure 2.2).

The self-consistent condition, that at a distance r from the cylinder axis every side chain occupies a surface area $\simeq \xi(r)^2$, with all the side chains together just covering the total cylinder surface $\simeq Lr$, has to be satisfied.

$$N\sigma\xi(r)^2 \simeq Lr \tag{2.1}$$

From this we obtain

$$\xi(r) \simeq r^{1/2}\left(\frac{a}{\sigma}\right)^{1/2} \tag{2.2}$$

The decreasing number of blobs as a function of r in a cross section parallel to the cylinder axis is given by

$$\frac{Na}{\xi(r)} \simeq Na^{1/2}\sigma^{1/2}r^{-1/2} \tag{2.3}$$

Whereas the increase in the number of blobs as a function of r in a cross-section perpendicular to the cylinder axis is given by

$$\frac{2\pi r}{\xi(r)} \simeq r^{1/2}(\sigma/a)^{1/2} \tag{2.4}$$

The application of the blob model described so far is illustrated in Figure 2.3 The density of segments $\rho(r)$ at a distance r from the cylinder axis is related to the diameter of the blob via the excluded volume statistics valid

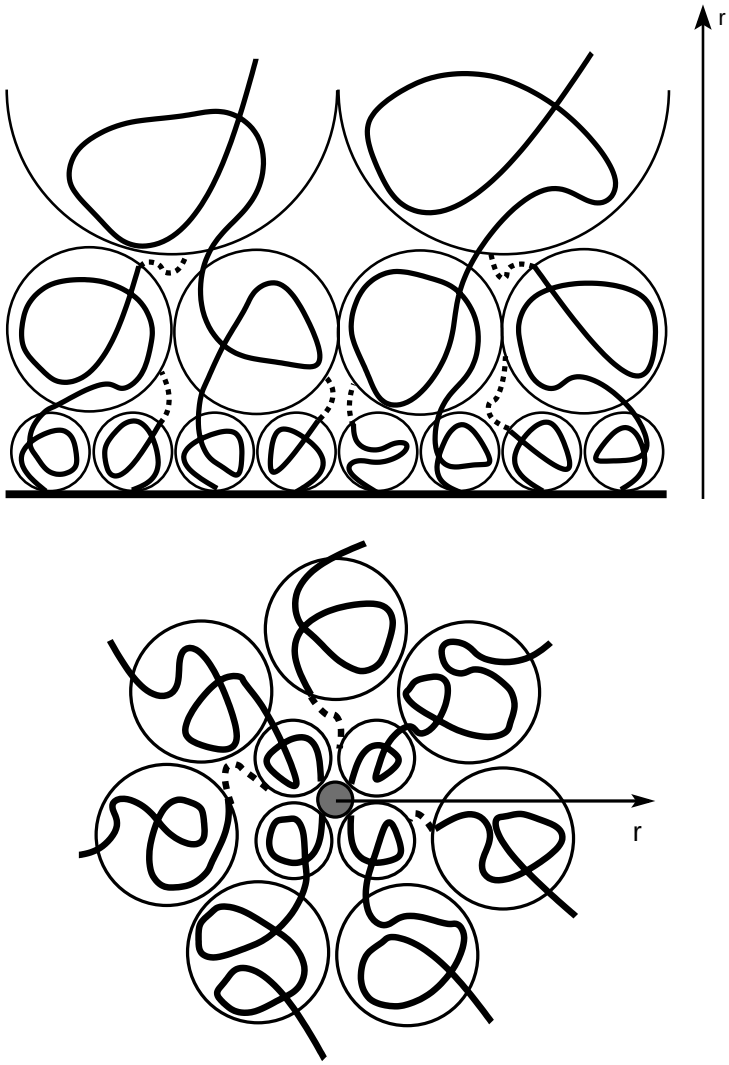

Figure 2.3: Top: illustration of decreasing number of blobs as a function of *r* in cross-section parallel to the cylinder axis. Bottom: illustration of increasing number of blobs as a function of *r* in cross-section perpendicular to the cylinder axis.

within a blob. The number of monomers g in a blob of size $\xi(r)$ satisfies $\xi(r) = ag^{3/5}$ (SAW statistics), hence

$$\rho(r) \simeq \frac{\xi(r)^{5/3}}{a^{5/3}\xi(r)^3} = a^{-5/3}\xi(r)^{-4/3} \tag{2.5}$$

If the radius of the cylindrical brush equals R, all the side chain segments just fill the cylinder, hence

$$N\sigma M \simeq L\int_0^R \mathrm{d}r\, r\rho(r) = a^{-5/3}L\int_0^R \mathrm{d}r\, r\xi(r)^{-4/3} \tag{2.6}$$

Combined with Eqn. (2.2) this gives

$$R \simeq a\sigma^{1/4}M^{3/4} \tag{2.7}$$

Note the typical 2*D Flory exponent* 3/4. We now assume that the backbone itself has no bending rigidity and the question arises whether a straight cylinderlike structure is stable and if true, over what distance. To address this we have to calculate the free energy of the brush as a function of bending. In the blob picture, each blob has an excess free energy of the order kT. Therefore, the free energy density $f(r)$ at a distance r for the straight brush is given by

$$f(r) \simeq \frac{kT}{\xi(r)^3} \tag{2.8}$$

The total free energy of the brush is accordingly

$$F \simeq kTL\int_0^R \mathrm{d}r\, \frac{r}{\xi(r)^3} \simeq NkT\sigma^{13/8}M^{3/8} \tag{2.9}$$

Per unit length this becomes

$$\frac{\beta F}{Na} \simeq \frac{\sigma^{13/8}M^{3/8}}{a} \tag{2.10}$$

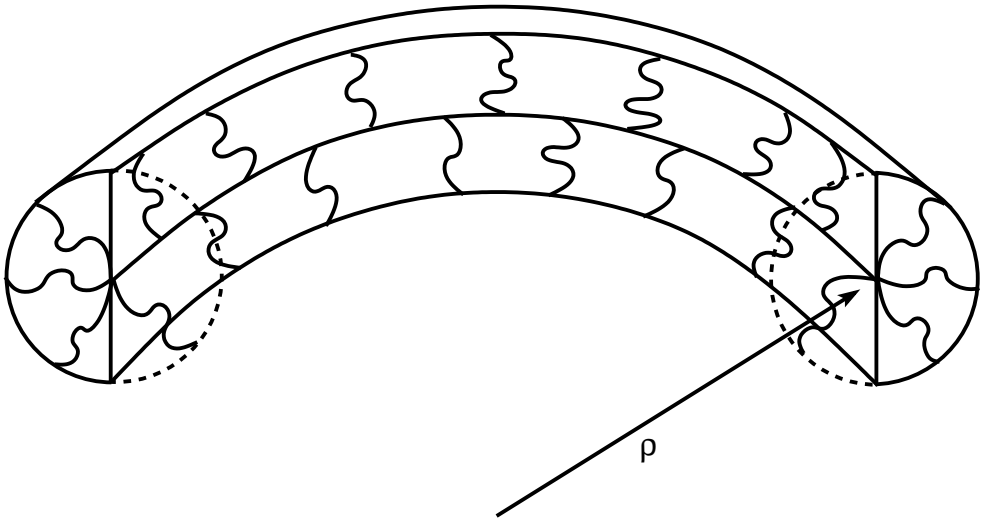

Figure 2.4: Illustration of a comb copolymer brush that is bending with a curvature radius ρ.

The increase in free energy upon bending with a radius of curvature ρ (Figure 2.4) for a persistent chain is directly related to the stiffness, i.e. persistence length λ [9, 15, 16]

$$\frac{\Delta F}{kT} \simeq \frac{\lambda}{\rho^2} \tag{2.11}$$

A somewhat more involved calculation shows that upon bending with a radius of curvature ρ the free energy can be expanded in terms of the curvature $1/\rho$ and is given by [7]

$$\frac{\beta F}{Na} \simeq \frac{\sigma^{13/8} M^{3/8}}{a} \left[1 + \frac{113}{490\pi^2} \left(\frac{R}{\rho} \right)^2 + \cdots \right] \tag{2.12}$$

Hence for the persistence length we find

$$\lambda \propto a\sigma^{17/8} M^{15/8} \tag{2.13}$$

With D scaling as R this means that the ratio λ/D satisfies

$$\frac{\lambda}{D} \propto \sigma^{15/8} M^{9/8} \tag{2.14}$$

Therefore the theory predicts that if the side chains are long enough the comb copolymer brush becomes very stiff, i.e. a real bottle-brush! Using a different approach, taking the elastic nature of the backbone into account, Birshtein and coworkers [5] derived a scaling relation slightly different from Eqn. (2.7)

$$D \propto M^{18/25} \sigma^{3/25} \tag{2.15}$$

In the same paper, the effect of the side chains on the local backbone extension, expressed in terms of the spatial distance between successive side chains l was derived

$$l \propto M^{3/25} \sigma^{-7/25} \tag{2.16}$$

As far as the persistence length is concerned, only a qualitative argument was given that $\lambda \propto D$. Subbotin and coworkers calculated the persistence length using a self consistent field rather than a scaling approach. Their result was that $\lambda \propto M^2$ and $\lambda/D \propto M^{5/4}$, confirming the conclusion of Fredrickson.

The quantitative approaches illustrate the role of the side chains in the stiffening of the structure and demonstrate that for sufficiently long side chains the persistence length should exceed the backbone length, thus resulting in a characteristic cylindrical comb copolymer brush structure. Furthermore, the backbone *expands* locally, however, the dependence of l on the side chain length M is relatively weak.

So far computer simulations, to be discussed in more detail in the next chapter, failed to demonstrate an increase of λ/D as a function of M. This may well be due to scaling arguments becoming valid only for much larger comb copolymer brushes than simulated so far. This complication is not present in the case of stiff side chains. This situation was first addressed by Subbotin and coworkers [10] who derived the following scaling relations

$$\frac{\lambda}{D} \propto M \tag{2.17}$$

$$l \propto M^0 \tag{2.18}$$

In terms of the characteristic length D, the increase in the persistence length as a function of the side chain length is very similar to that predicted for flexible side chains. The behavior of Eqn. (2.17) was indeed observed in the computer simulations. The spatial distance l between successive grafting points is now predicted to be independent of M, a result that was also shown to be in excellent agreement with computer simulations. Locally the backbone conformation continued to fluctuate strongly, independent of the length of the rigid side chains. Experimentally, the side chains are usually neither completely flexible nor rigid, hence also the behavior of l as a function of the side chain length is expected to be somewhere in between these two extremes. Based on the simulations one should expect tho find in practice a value of l that is much smaller than the maximum value corresponding to full extension (i.e. all-trans). An important conclusion from these simulations is that stiff side chains are far more effective stiffness inducing moieties than flexible side chains. This was further verified in a computer simulation study in which the stiffness of the side chains was systematically varied.

Since the stiffening is due to the excluded volume interaction between the side chains, the obvious next step is to consider $2D$ brushes where the excluded volume effect is much larger. Strikingly however, it turns out that this increased excluded volume effect may result in spontaneous curvature. Below we present a simple scaling argument investigating the bending instability. The same issue will be addressed by computer simulations in detail in Chapter 5.

Spontaneous curvature of the 2D bottle-brush

Recent theoretical work by Potemkin and coworkers [11, 17, 18] has demonstrated that the 2D molecular bottle-brush exhibits a bending instability when it is free to redistribute the side chains. This result was obtained based on mean field approximation. In this section we outline an alternative theoretical analysis incorporating the use of the blob model [6, 14] in the case of a comb copolymer brush strongly adsorbed to a flat surface. We will show that for bending instability to take place a requirement on the length of the side chains, or alternatively grafting density, has to be met.

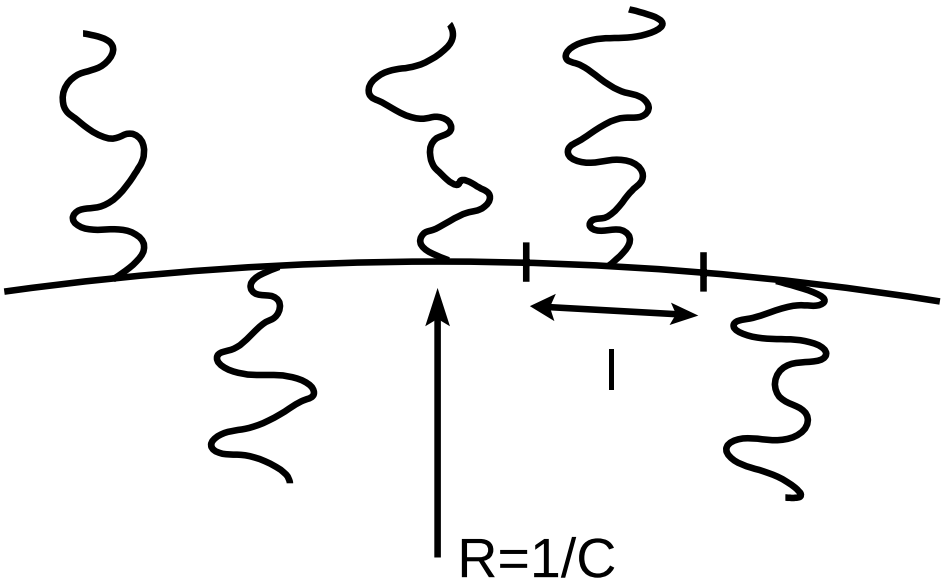

Figure 2.5: Schematic representation of a 2D comb copolymer showing a small bending.

Consider a infinitesimally small bending of the backbone, see Figure 2.5. We denote $\sigma = 1/l$ the grafting density, $C = 1/R$ curvature and M the number of segments in the side chains. The free energy upon bending can be expanded with respect to C ($lC \ll 1$). It is expressed as the free energy of the upper and lower part and the free energy of mixing for the side chain distribution. Let $\sigma_+ = \sigma^*(1 + p)$, where $\sigma^* = \sigma/2$, denote the grafting density of the upper part and similarly $\sigma_- = \sigma^*(1 - p)$ for the lower part. Then

$$\begin{aligned} F &= \mathcal{F}(\sigma_+) - \mathcal{H}(\sigma_+)C + \frac{1}{2}\mathcal{K}(\sigma_+)C^2 + \mathcal{F}(\sigma_-) + \mathcal{H}(\sigma_-)C + \frac{1}{2}\mathcal{K}(\sigma_-)C^2 \\ &\quad +\sigma^*[(1+p)\ln(1+p) + (1-p)\ln(1-p)] \end{aligned} \tag{2.19}$$

Here $\mathcal{F}(\sigma)$, $\mathcal{H}(\sigma)$ and $\mathcal{K}(\sigma)$ are expansion parameters depending on the model of the chain and interactions. For $p \ll 1$ the free energy can be expanded and minimized with respect to p. The mixing term does not

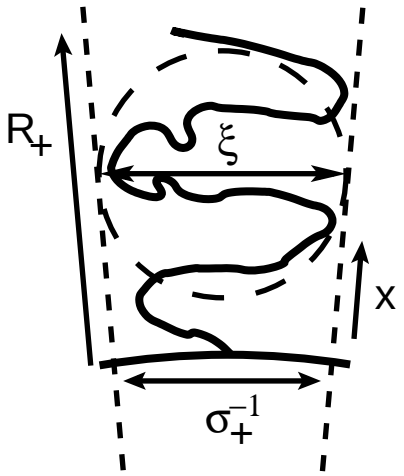

Figure 2.6: Schematic representation of the application of the 2D blob model.

contain any first order contribution, therefore the free energy is expanded up to second order

$$\begin{aligned} F &= 2\mathcal{F}(\sigma^*) + \mathcal{F}''(\sigma^*)\sigma^{*2}p^2 - 2\mathcal{H}'(\sigma^*)\sigma^* pC \\ &\quad +(\mathcal{K}(\sigma^*) + 1/2\mathcal{K}''(\sigma^*)\sigma^{*2}p^2)C^2 + \sigma^* p^2 \end{aligned} \tag{2.20}$$

Minimizing the free energy with respect to p gives

$$p = \frac{2\mathcal{H}'(\sigma^*)C}{2\mathcal{F}''(\sigma^*)\sigma^* + \mathcal{K}''(\sigma^*)\sigma^* C^2 + 2} \tag{2.21}$$

and for the free energy

$$F = 2\mathcal{F}(\sigma^*) + \left[\mathcal{K}(\sigma^*) - \frac{2\sigma^*\mathcal{H}'^2(\sigma^*)}{2 + 2\sigma^*\mathcal{F}''(\sigma^*) + \mathcal{K}''(\sigma^*)\sigma^* C^2}\right] C^2 \tag{2.22}$$

Hence, the change in the free energy upon bending (C small) can be written

$$\Delta F = \left[\mathcal{K}(\sigma^*) - \frac{\sigma^* \mathcal{H}'^2(\sigma^*)}{1 + \sigma^* \mathcal{F}''(\sigma^*)}\right] C^2 \tag{2.23}$$

When the factor between square brackets is negative, the free energy is lowered and there is an instability towards bending. We will now use scaling arguments to calculate the expansion parameters. Consider the situation in Figure 2.6 (the upper layer). For the size of a blob at a distance x from the backbone the correlation length is given by

$$\xi(x) = \sigma_+^{-1}(1 + Cx) = am^\nu \tag{2.24}$$

Here a is the statistical segment length, m is the number of segments per blob and ν is the scaling exponent (for a SAW in 2D $\nu = 3/4$). The density of segments satisfies

$$\rho(x) \simeq \frac{m}{\pi \xi(x)^2} = \frac{1}{\pi a^{1/\nu}} \sigma_+^{\frac{2\nu-1}{\nu}} (1 + Cx)^{\frac{1-2\nu}{\nu}} \tag{2.25}$$

The free energy per blob equals kT, so the 2D free energy density we have

$$f(x) \simeq kT/\xi(x)^2 \tag{2.26}$$

In order to relate the total number of segments per side chain M to the end to end point distance R_+ we expand $\rho(x)$ and integrate giving

$$\begin{aligned} M &= \frac{1}{\sigma_+} \int_0^{R_+} \mathrm{d}x (1 + Cx)\rho(x) \\ &= \frac{1}{\pi}\left(\frac{1}{a\sigma_+}\right)^{\frac{1}{\nu}} \frac{\sigma_+}{C}\left[(CR_+) + \frac{1-\nu}{2\nu}(CR_+)^2 + \frac{(1-\nu)(1-2\nu)}{6\nu^2}(CR_+)^3\right] \end{aligned} \tag{2.27}$$

We require CR_+ in order to substitute its value into the integration of the free energy. We employ perturbation theory to obtain the value of CR_+. Consider the general case of a third order polynomial with a small constant term

$$x + ax^2 + bx^3 = \epsilon \tag{2.28}$$

Since ϵ is small, so will the root closest to zero be. We may expand this root in terms of ϵ

$$x_0 = \epsilon + p\epsilon^2 + q\epsilon^3 \tag{2.29}$$

Substituting the expansion into the polynomial equation and solving for p and q we obtain

$$x_0 = \epsilon - a\epsilon^2 + (2a^2 - b)\epsilon^3 \tag{2.30}$$

Therefore we find that

$$\begin{aligned} CR_+ &= \frac{\pi MC}{\sigma_+}(\sigma_+ a)^{1/\nu} - \frac{1-\nu}{2\nu}\left[\frac{\pi MC}{\sigma_+}(\sigma_+ a)^{1/\nu}\right]^2 \\ &+ \frac{(1-\nu)(2-\nu)}{6\nu^2}\left[\frac{\pi MC}{\sigma_+}(\sigma_+ a)^{1/\nu}\right]^3 \end{aligned} \tag{2.31}$$

We subsequently substitute this value into the integration of the free energy to find the free energy per unit length (in units of kT)

$$\begin{aligned} F &= \int_0^{R_+} \mathrm{d}x(1+Cx)f(x) \\ &\approx \sigma_+^2 \int_0^{R_+} \mathrm{d}x(1 - Cx + C^2x^2) \\ &= \frac{\sigma_+^2}{C}\left[(CR_+) - \frac{(CR_+)^2}{2} + \frac{(CR_+)^3}{3}\right] \\ &= \frac{\pi M}{a}(\sigma_+ a)^{(1+\nu)/\nu} - \frac{\pi^2 M^2}{2\nu}(\sigma_+ a)^{2/\nu}C + \frac{\pi^3 M^3 a}{3\nu^2}(\sigma_+ a)^{(3-\nu)/\nu}C^2 \\ &= \mathcal{F}(\sigma_+) - \mathcal{H}(\sigma_+)C + \frac{1}{2}\mathcal{K}(\sigma_+)C^2 \end{aligned} \tag{2.32}$$

After substitution of the expansion parameters in equation (2.23) we find that the 2D brush is stable, i.e. does not curve spontaneously, for $\nu > 1/2$. This result is consistent with the computer simulations of Saariaho and coworkers [19].

Formally, the free energy (2.23) becomes negative for $\nu < 1/2$. However, in that case the correlation length of the side layer $\xi > (\sigma^*)^{-1}$, and the scaling approach is not acceptable. A mean field approach should be employed now and this shows the 2D brush to be unstable with respect to bending. Entering the second virial coefficient $B = v(1-2\chi)$ of the segment interaction [20], where v is the excluded volume of the segment and χ is the Flory parameter, the correlation length is given by

$$\xi \simeq a^2 / \sqrt{v(1-2\chi)} \tag{2.33}$$

Using Potemkins results [17] and taking into account the mixing entropy of the side chains, we find the minimal side chain length for which instability towards bending occurs

$$M > M^* \simeq \left(\frac{a}{v\sigma}\right)^{2/3} \frac{1}{(1-2\chi)^{2/3}} \tag{2.34}$$

The requirement on the grafting density in this case is

$$\sigma a > \sqrt{(v/a^2)(1-2\chi)} \tag{2.35}$$

We conclude that additional repulsion between side chain segments may stabilize the 2D brush with respect to bending. The requirement above, on the minimal length of the side chains, is the result of a rather lengthy calculation, but it can also be obtained using simple arguments. Consider the situation in Figure 2.7. The elastic energy of the side chains equals

$$E = \frac{1}{a^2}\int_0^M \mathrm{d}n \left(\frac{\mathrm{d}x}{\mathrm{d}n}\right)^2 = \frac{1}{a^2}\int_0^R \mathrm{d}x \left(\frac{\mathrm{d}x}{\mathrm{d}n}\right) = \frac{R\sigma}{a^2\phi} \tag{2.36}$$

Here ϕ is the concentration and the stretching of the side chains is assumed to be constant. Adding the second virial coefficient the free energy per unit length becomes

$$F = \frac{R\sigma^2}{a^2\phi} + \frac{w}{2}R\phi^2 \tag{2.37}$$

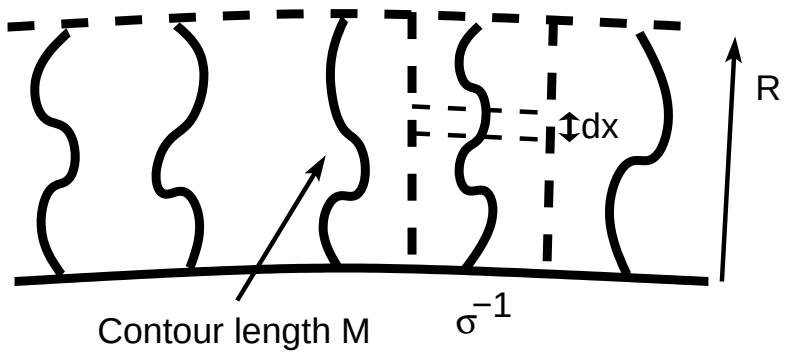

Figure 2.7: Schematic representation of a 2D comb and model parameters.

Minimizing with respect to ϕ gives

$$\phi = \left(\frac{\sigma^2}{a^2 w}\right)^{1/3} \tag{2.38}$$

and for the free energy

$$F \simeq \frac{w^{2/3} M \sigma^{5/3}}{a^{2/3}} \tag{2.39}$$

The free energy of mixing per unit length in units of kT equals $F_{mix} = \sigma$. When $F > F_{mix}$, the free energy of mixing cannot stabilize the comb copolymer brush and when replacing w by its proper value Equation (2.34) is obtained. The analysis of the 2D comb copolymer brush clearly demonstrates that spontaneous curvature is a very subtle effect. A computer simulation study on this matter is presented in Chapter 5.

References

[1] B. Zimm, W. Stockmayer, *J. Chem. Phys.* **1949**, *17*, 1301.

[2] O. Ptitsyn, *J. Phys. Chem. USSR* **1955**, *29*, 396.

[3] A. Kron, O. Ptitsyn, *Vysokomolekul. Soedin.* **1963**, *5*, 397.

[4] G. Berry, O. T.A., *J. Chem. Phys.* **1963**, *40*, 1614.

[5] T. Birshtein, O. Borisov, Y. Zhulina, A. Khokhlov, T. Yurasova, *Polymer Science USSR* **1987**, *29*, 1293.

[6] Z. Wang, S. Safran, *J. Chem. Phys.* **1988**, *89*, 5323.

[7] G. Fredrickson, *Macromolecules* **1993**, *26*, 2825.

[8] Y. Rouault, O. V. Borisov, *Macromolecules* **1996**, *29*, 2605.

[9] A. Subbotin, M. Saariaho, O. Ikkala, G. ten Brinke, *Macromolecules* **2000**, *33*, 3447.

[10] A. Subbotin, M. Saariaho, O. Ikkala, G. ten Brinke, *Macromolecules* **2000**, *33*, 6168.

[11] I. Potemkin, A. Khokhlov, P. Reineker, *Eur. Phys. J. E* **2001**, *4*, 93.

[12] R. Stepanyan, A. Subbotin, G. ten Brinke, *Phys. Rev. E.* **2001**, *63*, 61805.

[13] R. R. Stepanyan, A. Subbotin, G. ten Brinke, *Macromolecules* **2002**, *35*, 5640.

[14] M. Daoud, J. Cotton, *J. Phys. (Paris)* **1982**, *43*, 531.

[15] T. Odijk, *J. Polym. Sci. Polym. Phys. Ed.* **1977**, *15*, 477.

[16] J. Skolnick, M. Fixman, *Macromolecules* **1977**, *10*, 944.

[17] I. Potemkin, *Eur. Phys. J. E* **2003**, *12*, 207.

[18] I. Potemkin, A. Khokhlov, S. Prokhorova, S. Sheiko, M. Möller, K. Beers, K. Matyjaszewski, *Macromolecules* **2004**, *37*, 3918.

[19] M. Saariaho, O. Ikkala, G. ten Brinke, *J. Chem. Phys.* **1999**, *110*, 1180.

[20] P. G. de Gennes, "*Scaling concepts in polymer physics*", Cornell University Press, Ithaca 1985.

3

Simulations of Cylindrical Polymer Brushes

Monte Carlo simulation

In this section some of the basics of Monte Carlo simulations in general and the application to polymer systems will be discussed.

Monte Carlo

The Monte Carlo method is not strictly limited for use in simulations. In fact, any method involving a random element in order to perform an evaluation could be considered a Monte Carlo method. As an example, consider the estimation of π by a Monte Carlo method. For a quadrant of the unit circle the area equals $A = \pi/4$, see Figure 3.1. When a pair of random numbers is generated, both in the range $x, y \in [0, 1]$, these represent a randomly selected point on the indicated unit square. The probability that this point will lie inside the circle segment is equal to the ratio of the areas of the circle quadrant and the unit square, i.e. $\pi/4$. If N such pairs are generated and for I of those it holds that $\sqrt{x^2 + y^2} \leq 1$, than an estimate for π is given by $\pi \approx 4 \times I/N$.

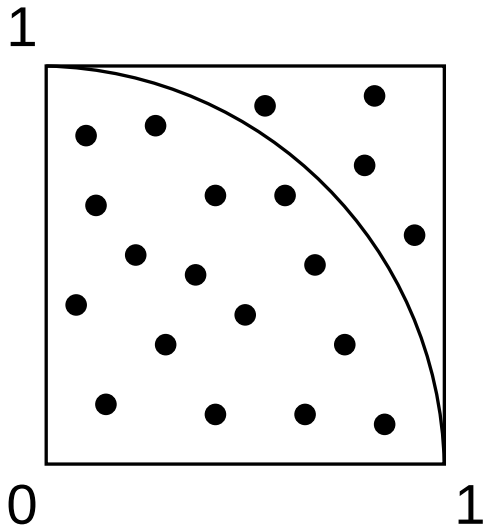

Figure 3.1: Calculating the value of π using a Monte Carlo method.

As every generated pair forms an independent measurement the statistical error in the evaluation of π is expected to be $4/\sqrt{N}$. This means that a modern computer generating random number pairs for a period of the order of the age of the universe would hardly be able to get more than 15 decimals of accuracy. In this case the Monte Carlo method is not particularly efficient. However, it is not always possible to construct efficient numerical methods and often in polymer science relative errors of 5% or less are sufficient to detect e.g. a power law dependence between observables.

In most cases the problem from a statistical point of view is not so much about obtaining a sufficient amount of values but the statistical independence and relevance (statistical weight) of these values. Very illustrative in this context is the example of measuring the average depth of the Nile as discussed in the book by Frenkel and Smit [1]. One could generate a number of coordinates all over Africa and measure the depth of the Nile at that position. However, most of these points would not actually be *in* the Nile and hence the statistical weight of the corresponding measurement would be zero. It would be a lot more efficient if the probability distribution for positions inside the Nile could somehow be incorporated into the sampling method. In this case the solution is trivial: Only take measurements at locations in the Nile. We will next discuss some statistical mechanics and how the efficiency of the sampling method can be increased.

Statistical Mechanics

The classical partition function for a system of N particles is given by

$$Q = c \int \mathrm{d}p^N \mathrm{d}r^N \exp[-\mathcal{H}(r^N p^N)/k_B T] \tag{3.1}$$

Here r^N and p^N are the positions and momenta of all particles and $\mathcal{H}(r^N p^N)$ is the Hamiltonian. Usually we are interested in obtaining averages of observables in equilibrium that depend only on the positions of the particles, i.e. static configurational properties. In this case we consider the configurational part of the partition function only and write

$$Z \equiv \int \mathrm{d}x \exp[-\beta U(x)] \tag{3.2}$$

where x denotes the configurational state of the system and $U(x)$ denotes the potential energy. Monte Carlo simulations on systems of N particles probe the canonical ensemble, i.e. the temperature T, the volume V and the number of particles N remains constant. In equilibrium the distribution of states satisfies Boltzmann statistics and for the thermodynamic average of an observable we may write

$$\langle A \rangle_{N,V,T} = \frac{\int \mathrm{d}x\, A(x) \exp[-\beta U(x)]}{\int \mathrm{d}x \exp[-\beta U(x)]} \tag{3.3}$$

In the vast majority of cases the integrals cannot be evaluated analytically and often it is not feasible to compute values numerically. However, it may be possible to get a good approximation by taking a subset of a finite number of states and convert the integration to summation

$$\langle A \rangle_{N,V,T} \simeq \frac{\sum^{n} A(x_i) \exp[-\beta U(x_i)]}{\sum^{n} \exp[-\beta U(x_i)]} \tag{3.4}$$

where n denotes the total number of sampled states. Increasing the number of samples increases the accuracy. However, as in the Nile example, simple sampling by choosing random configurations in phase space will generate a lot of samples with negligible Boltzmann factor. It is much more efficient to use the Metropolis scheme also known as importance sampling. The basic idea is to generate points in configuration space with a relative probability proportional to the Boltzmann factor. That way weighted averaging is converted into simple averaging and the sampling efficiency is increased as well. Next we will consider how to setup a Monte Carlo scheme that satisfies this property.

Metropolis Monte Carlo

The general idea of the Metropolis Monte Carlo scheme is to set up a stochastic Markov process, resulting in a set of correlated samples that satisfy the Boltzmann distribution. In practice this means that a certain configurational state is generated that serves as the starting condition and that subsequent states are generated by introducing small deviations from

the previous state. Of key importance here is the fact that the change is not accepted unconditionally, but rather with a certain transition probability π_{xy}. The transition probability between two states x and y must be chosen in such a way that any state can be reached from any other state in a finite number of steps. This condition is called *ergodicity*. In addition, the transition probability should not destroy the equilibrium distribution and hence the average number of accepted moves that leave a certain state x should be equal to the average number of accepted moves from all other states to x or

$$\sum_{x \in S} \rho_x \pi_{xy} = \rho_y \tag{3.5}$$

Here ρ_x denotes the relative probability for the system to be in state x. However, it is more convenient to impose the stronger *detailed balance* condition that the average number of accepted moves from x to any other state y is equal to the number of reverse moves

$$\rho_x \pi_{xy} = \rho_y \pi_{yx} \tag{3.6}$$

The transition probability can be written as $\pi_{xy} = \alpha_{xy} p_{xy}$ where α_{xy} is the probability that a move from state x to state y is attempted and p_{xy} is the probability for acceptance. Usually α_{xy} is chosen to be symmetric and therefore Eqn. (3.6) yields

$$\frac{p_{xy}}{p_{yx}} = \frac{\rho_y}{\rho_x} = \exp[-\beta(U_y - U_x)] \tag{3.7}$$

There is more than one choice for p_{xy} possible, but originally Metropolis and coworkers [2] set the probability for a trial move that lowers the energy to be accepted to 1 and so

$$p_{xy} = \min\{1, \exp[-\beta(U_y - U_x)]\} \tag{3.8}$$

It is of vital importance that after a move has been rejected the last sample is once again taken into account in the statistics. Failure to do so may lead to biased statistics. This can be illustrated by performing a thought Monte Carlo experiment. Consider a particle on a one dimensional lattice. We impose a potential that is zero on $i \in [-1, 1]$ and infinite elsewhere. Classically, the probability distribution is trivial: The particle exists with

equal probability at either of the three positions with zero potential and with zero probability elsewhere.

Let us perform a simulation starting with the particle in a randomly chosen 'allowed' box. We introduce only one kind of Monte Carlo move that displaces the particle randomly to one of the neighboring sites. After rejecting a move we do no re-sample but perform a new move first. This means that if the particle is at position $i = -1$ or $i = 1$ the next sample will always find the particle at position $i = 0$, i.e. $\pi_{-1,0} = \pi_{1,0} = 1$, $\pi_{0,-1} = \pi_{0,1} = 1/2$ and all other transition probabilities are zero[1]. Using the stationary condition Eq. (3.5) we find that $\rho_{-1} = \rho_1 = 1/2\rho_0$, which is in disagreement with Boltzmann statistics. If now, after a rejection, we do take the last sample into account we have: $1/2 = \pi_{-1,-1} = \pi_{-1,0} = \pi_{0,-1} = \pi_{0,1} = \pi_{1,1} = \pi_{1,0}$. In this case, using the stationary condition, we find that $\rho_{-1} = \rho_0 = \rho_1$.

One of the drawbacks of the Metropolis Monte Carlo method is that consecutive conformations are correlated. This means that the number of statistically independent samples is in general much smaller than the total number of samples. Also, since the starting conformation in most cases is constructed artificially a number of samples at the beginning of the simulation run must be omitted from statistics in order to ensure that the averaging starts at a point statistically independent from a starting conformation that may find the system far from thermodynamic equilibrium. This process is called *equilibration*.

The Bond Fluctuation Model

Polymers can be modelled as chains of beads connected together. When the orientation of consecutive bonds between beads is limited by excluded volume only, the beads can be interpreted as Kuhn segments for linear chains. The models used for simulation purposes are divided into two categories: lattice models and off-lattice models. In the latter case the segment position vectors exist in continuous space. This discussion will be limited to the case of the bond fluctuation model (BFM) a lattice model in which the segment position vectors reside on a lattice.

[1] These are relative, unnormalized probabilities.

In contrast to most other lattice models beads in the BFM occupy more than one lattice site, 2^D to be precise with D being the number of dimensions. In the 3-dimensional BFM these lattice sites form a cube and a fixed, and consistent for all beads, choice of one of these sites can serve as the position vector. A bond between two successive beads may have a fluctuating length. Usually, the set of allowed bond vectors is limited to those that satisfy entanglement constraints, i.e. bonds cannot pass through each other. Due to excluded volume the smallest bond length equals 2 and bond lengths ≥ 4 do not satisfy entanglement constraints. Let $P(i, j, k)$ denote the set of all permutations of $\pm i$, $\pm j$ and $\pm k$, then the following bond vectors satisfy the requirements

$$\vec{b} = P(2,0,0), P(2,1,0), P(2,1,1), P(3,0,0) \tag{3.9}$$

Only one trial move exists in the BFM: displacing a random bead with one lattice spacing. Because of this there exist a number of bond vectors that can be reached from (3.9) which do not result in bond crossing. By adding the vector $P(1,0,0)$ to (3.9) we get

$$\vec{b} = P(2,2,0), P(2,2,1), P(3,1,0), P(3,1,1) \tag{3.10}$$

However, these vectors should be reached from (3.9) only. Based on bond length and spherical symmetry of the set of possible bond vectors the set $P(2,2,1)$ and $P(3,1,0)$ is chosen which completes the final set

$$\vec{b} = P(2,0,0), P(2,1,0), P(2,1,1), P(2,2,1), P(3,0,0), P(3,1,0) \tag{3.11}$$

In other words: A bond vector is allowed when its length is $b \in [2, \sqrt{10}] \setminus \sqrt{8}$ The set of allowed bond vectors contains 108 elements with 5 different bond lengths. There are 100 different possible bond angles between $[0, \pi\rangle$ of which the largest 13 are prohibited due to excluded volume constraints. This is a large improvement on the possibilities provided by single site lattice models. In the 2-dimensional case the allowed bond vectors belong to the set $b \in [2, \sqrt{13}]$. Figures 3.2 and 3.3 show the allowed set of bond vectors and the application of a trial move on a chain respectively.

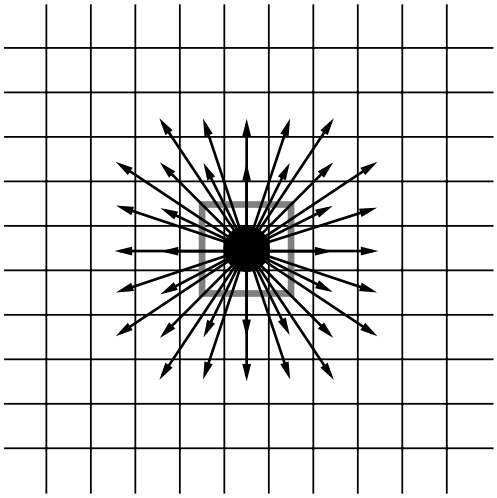

Figure 3.2: Schematic representation indicating the allowed positions for beads bonded to the central indicated bead.

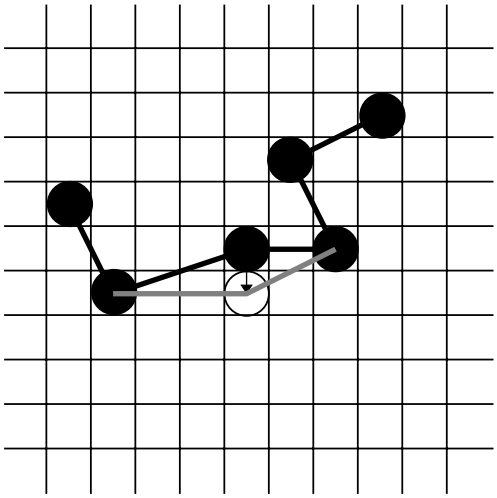

Figure 3.3: Schematic representation of the trial move in the bond fluctuation model.

The, obviously not optimized, algorithm of the 3 dimensional BFM expressed in pseudo C code proceeds as follows

```
for(i = 0; i < NMoves; i++) {
        SampleConformation();
        energy = CalculateEnergy();
        bead = N * random();
        direction = 6 * random();
        for(j = 0; j < 8; j++) {
                MoveSite(bead, j, direction);
        }
        for(j = 0; j < 8; j++) {
                if(ExcludedVolumeViolated(bead, j)) {
                        rejected = true;
                }
        }
        if(rejected == true) {
                for(j = 0; j < 8; j++) {
                        MoveSite(bead, j, -direction);
                }
                nextloop;
        }
        if(BondlengthsNotOk(bead)) {
                for(j = 0; j < 8; j++) {
                        MoveSite(bead, j, -direction);
                }
                nextloop;
        }
        energychange = CalculateEnergy() - energy;
        boltzman = exp(-energychange);
        diceroll = 1.0 * random();
        if(diceroll > boltzmann) {
                for(j = 0; j < 8; j++)
                        MoveSite(bead, j, -direction);
        }
```

The infinite lattice approach

For our first publication that made use of the BFM for simulating comb copolymer brushes [3] we developed what we call the 'infinite lattice approach'. Usually, when performing simulations of the melt, a simulation box of finite dimensions $l \times w \times h$ is chosen containing lwh lattice sites. This box is thought of as being representative for a sufficiently large volume of the, in principle, infinite melt. As such the infinite melt consists of an infinite number of the same simulation box with the same configurational state that are linked together. This is fine as long as the simulation box is large enough to contain a sufficiently large number of molecules. Such an approach requires periodic boundary conditions at the edges of the box, meaning that monomers that get moved out of the box re-enter the box at the opposite side. Intuitively, this is what one should expect since the number of segments in the box should be preserved. Periodic boundary conditions in this case mean also that segments near opposite sides of the simulation box interact with each other if the distance between one segment and the periodic image of the other is within the range of the potential.

When single polymer chains in infinitely dilute solution are being simulated the size of the polymer is usually much larger than in the melt. Using a simulation box with periodic boundary conditions one has to make certain that the box is large enough that the polymer does not 'feel' itself. Monomers that leave the box at one edge should still interact with the monomers on the other side, however they should not interact with monomers on the same side that are possibly part of the other side of the polymer chain. This is generally dealt with by taking a very large simulation box. However, as the required amount of memory scales as the third power of the simulation box size this can put serious limitations on the size of the systems that can still be investigated.

The infinite lattice approach still makes use of a finite lattice. However, positions outside that lattice are mapped back into the finite box, preserving their 'real' coordinate in memory as well. The lattice sites in the finite box contain a list of monomers that occupy that site. This list may be empty, but can also be used by an indefinite amount of chain segments. Since the real coordinate of the segments is preserved as well, it is quite straightforward to find out if two monomers should interact or not. As

far as the polymer is concerned it exists on an infinite lattice although the simulation box in computer memory is finite. The simulation results are completely independent of the size of the simulation box. Therefore it is possible to simulate very large polymers on computers with a low to medium amount of memory, since the required amount of memory scales as the number of beads N rather than the number of lattice sites L^3. The only disadvantage of choosing a very small simulation box is the increase of 'bookkeeping' overhead. In the case of choosing a $1 \times 1 \times 1$ lattice the situation of an off-lattice model is reached, except from the fact that the position coordinates are discretized.

Figure 3.4 shows the part of an infinite 2-dimensional lattice on which a polymer conformation resides. The pictures on the right hand side of the figure show two possibilities for the choice of a simulation box that is smaller than the polymer itself. The numbers inside the beads indicate occupation numbers, i.e. the amount of beads from different periodic images that occupy the same position in the simulation box. Note however, that every bead occupies 4 lattice sites, which are the corners of every white square. Therefore the number of beads actually making use of a certain lattice site is the sum of the numbers inside the beads in the squares that border the lattice site itself. In the trivial case of the 2×2 lattice this means that the occupation number of the central site in this example is always $N = 16$.

Simulations of cylindrical polymer brushes: a review

Long before the first successful polymerization of macromonomers by Tsukahara and coworkers [4–6] in the late 80's of the previous century the effects of branching on the conformational properties of polymers had been discussed in a number of theoretical papers [7–10] (in the late 40's through mid 60's). At that point computer hardware and simulation methods caught up with theory which resulted in the first simulation study, based on the regular comb model, by Gallacher and Windwer [11]. In this particular study a Monte Carlo procedure was used in which conformations were generated on a tetrahedral lattice. The backbone consisted of 200 steps and the side chains varied in length from 3 to 7 steps. The spacing between grafts was varied from 4 to 10. Despite the rather short side chains, too short to

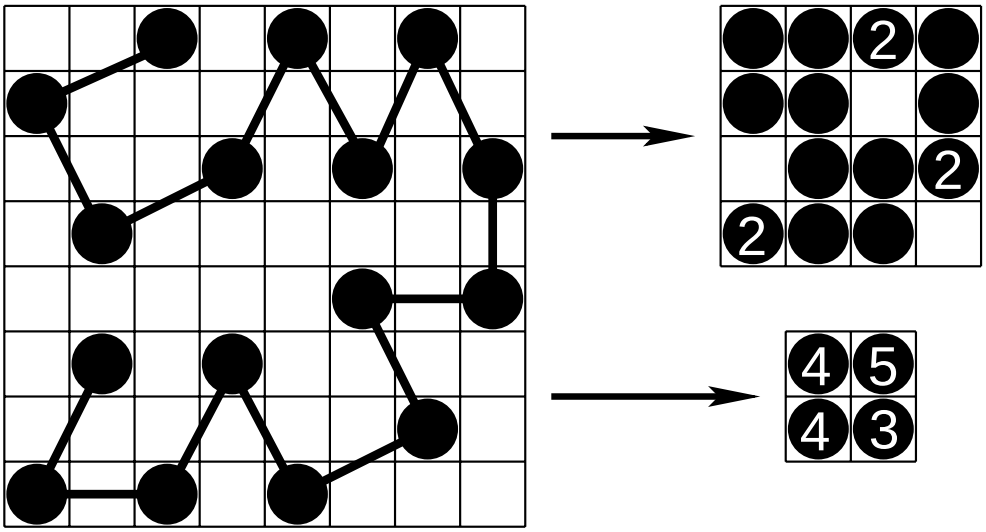

Figure 3.4: Illustration of the use of an infinite lattice. Left: part of an infinite lattice with a polymer conformation. Right: two possible ways of storing the conformation on a finite lattice. Numbers represent occupation values.

display accurate self-avoiding walk (SAW) statistics, pronounced excluded volume effects were observed. It was found that branched polymers have higher expansion factors in good solvent than linear polymers and that the expansion factor increases with both side chain length and grafting density. Moreover, when the side chains were short and few the size of the polymers were found to scale similar to linear polymers, i.e. obeying SAW statistics. With increasing side chain length and grafting density however, the scaling exponent was found to increase considerably. For the most densely grafted system with side chain length 5 and spacing 4 both the squared radius of gyration and the squared end-to-end-point distance showed a scaling exponent exceeding a value of 1.3.

Although by modern standards the values of the side chain parameters were by no means striking, the size of the backbone was considerable. It is very likely that the fact that it took fifteen years for another thorough simulation study of single comb branched polymers to be published cannot be attributed to lack of interest alone. In their 1981 simulation study,

McCrackin and Mazur [12] employed the Rosenbluth-Rosenbluth method to generate self avoiding walks on a cubic lattice. In addition to excluded volume interactions an attractive potential between non-bonded segments was introduced. In this way the solvent conditions for the simulated systems could be varied and the strength of the potential corresponding to θ-solvent conditions for linear chains was used for the θ point of the branched systems as well. The number of branches was varied between 5 and 30 and the ratio of the length of the side chains to the backbone length between 0 and 3. For the 10 branch comb copolymers the total number of segments reached 1650. For the simulated architectures the ratio

$$g = \frac{\langle R_g^2 \rangle_b}{\langle R_g^2 \rangle_l} \tag{3.12}$$

with $\langle R_g^2 \rangle_b$ and $\langle R_g^2 \rangle_l$ the mean-square radius of gyration of a branched polymer and a linear polymer with equal molecular weight respectively, was calculated. At the θ point this ratio was found to be weakly dependent on N, the total number of segments, and extrapolated to infinity. g_θ increased with the number of branches and was found to be larger than values calculated by the random walk model of the polymer.

The expansion factors of the comb-branched polymers were also calculated at the θ point. In contrast to the predictions of the self avoiding walk model, the expansion factors of the branched architectures were found to be smaller instead of greater than those of their linear counterparts. Here the square of the expansion factor was defined as the ratio of the radius of gyration squared in a given solvent quality and the radius of gyration squared in theta solvent. The authors concluded that the swelling of polymers in good solvent, when compared to a θ solvent, is diminished by the presence of branches. In addition, it was found that the radius of gyration of the backbone was always larger than that of a linear polymer of equal length even at θ temperature. This effect increased with both side chain length and the number of branching points. The random walk model predicts the radii of gyration to be equal at the θ point. The authors suggested that the random walk model may not be suitable for describing branched polymers in dilute solution under θ conditions.

Again, following the work of McCrackin and Mazur there has been a large gap in which the work on branched polymers was dominated by the

same group of authors often appearing together in various combinations on several papers [13–19]. The architectures discussed in these works include uniform stars, H-combs, and brushes having two branching points to which more than one side chain may be grafted. In the early 90's Bishop and Saltiel contributed simulation studies on H-combs in two and three dimensions [20, 21]. All of these studies investigated the influence of branching on the conformational properties of polymers such as expansion parameters and size scaling, but the first work to re-address regular combs was published in 1991 by Lipson [22]. The architectures that were investigated were divided in three categories by the ratio of side chain length to the distance between grafts (3/10, 6/6, and 9/4). The simulations were performed by generating SAWs on a tetrahedral lattice. The main findings of this study were that the Gaussian model underestimates the g-ratio as defined in Eqn. 3.12 and that the scaling of the radius of gyration versus the molecular weight deviates from SAW statistics. The author suggested that in the asymptotic limit SAW statistics should be retained, but that finite size effects cannot be neglected in contrast to what is the case for e.g. uniform stars. Gauger and Pakula [23] published results for comb copolymers in dilute solution as well as in the melt. Their main result was that the molecular architecture affects the side chains only in two dimensions and in three dimensional solutions. In three-dimensional melts they remain randomly coiled. The authors suggested that this result could be related to screening of the excluded volume interaction.

The first study that compared Monte Carlo results with scaling predictions from theory was published by Rouault and Borisov in 1995 [24]. The bond fluctuation model (BFM) was employed to study the scaling behavior of comb copolymer brushes in dilute solution. Comb-like polymers were considered with a main chain length of 200 and 800 segments. The length of the side chains were varied as well as the grafting density. The grafting density in this study was never so high that the spacers between side chains effectively vanished. Even when the ratio of side chain length to spacer length reached 4 the conformations of side chains and spacers differed only slightly from SAW statistics. On intermediate and long length scales however the conformation of the backbone was affected significantly, provided the side chains were sufficiently long. The backbone showed partial stretching on the length scale of several spacers as well as correlations in

the orientation of end-to-end vectors of the corresponding parts of the backbone. For the longest side chains there was a rapid increase in the dimensions of the comb in agreement with scaling theory. However, no statements were made about whether even higher grafting densities or side chain lengths would be able to make the polymer behave like a stiff cylindrical object. Later Rouault [25] reported a simulation study on similar comb copolymer brushes for which attraction between side chains was introduced. This attraction resulted in a transition from comb polymers to polysoaps, an effect that had been observed in experiment. Not only was the association of polymer molecules observed, but single chains displayed polysoap behavior as well.

A large body of work on the scaling of comb copolymer brushes as well as on the effect of side chains on overall stiffness of bottle-brush molecules was reported in five papers by Saariaho and coworkers [26–30]. In the first of these publications an off-lattice Monte Carlo study was presented of single bottle-brush polymer molecules in good solvent. The largest structure that was simulated consisted of a backbone of 100 segments to which 50 side chains with a length of 20 segments were attached. A smaller system with a backbone of 50 segments carried the same amount of side chains. This introduced a considerably higher grafting density when compared to previous simulation studies. For all structures the persistence length λ was evaluated. In addition, the eigenvalues of the gyration tensor of the molecule were calculated in order to characterize the shape. The persistence length was found to scale with side chain length with an exponent of 0.7, which is completely at odds with the value of 1.9 predicted by Fredrickson [31]. The behavior of the radio λ/D, with D denoting the brush diameter, was also at variance with the predictions of Fredrickson. In fact, while Fredrickson predicted the ratio to increase with side chain length, the simulation results showed it to level off. The original analysis of Birshtein and Borisov [32] did predict the ratio to become independent of side chain length. An analysis of the eigenvalues of the gyration tensor showed that upon increasing the side chain length the shape of the molecule deviates more and more from spherical. However, since the persistence length remained less than twice the brush diameter no clear cylindrical structures were formed. The simulation results appeared to be at variance with experimental results in which lyotropic behavior was observed for polymacromonomers. The authors

pointed out however that in the experimental case the monomers of the side chains were significantly larger than those of the backbone. Moreover, the stiffness of the backbone and the side chains was much larger than for the freely jointed model that was being used in the simulation study. The authors concluded that it should be possible to obtain lyotropic behavior by altering the side chain topology.

In the subsequent study [27] the same architectures were investigated, but the ratio of the size of the side chain beads and the backbone beads was varied between 1 and 3. Again, the ratio between the persistence length and the brush diameter was found to be virtually independent of side chain length. However, the ratio increased considerably with side chain bead size. This confirmed the importance of side chain topology and the authors concluded that in this way it might be possible to increase the ratio of persistence length and brush diameter enough to obtain lyotropic behavior.

The next logical step was to consider the dependence of the stiffness of molecular bottle-brushes on side chain rigidity. In their third work [28] Saariaho and coworkers performed simulations on comb copolymer brushes with a backbone consisting of up to 300 segments to which 150 side chains were grafted with up to 80 segments. All architectures were simulated as single chains in dilute solution with good solvent. The side chains were either fully flexible or completely rigid. A most striking observation was that the presence of rigid side chains did not influence the local backbone structure. Flexible side chains always induce a local stretching of the backbone, however rigid side chains affect the conformational behavior of the comb at longer length scales only. Apparently, the comb copolymer brushes need to be characterized at two length scales. At large length scales the persistence length of the combs with rigid side chains was considerably larger than for those with flexible side chains. In addition, in the case of rigid side chains the ratio λ/D was found to increase linearly with side chain length, whereas in the case of flexible side chains this ratio was, again, found to be virtually independent of side chain length. The authors concluded that rigid side chains are far more effective in obtaining stiff cylindrical brushes than flexible side chains. The results were compared with experimental findings in which large persistence lengths had been observed. The suggestion that this may be due to the semi-flexible nature of the side chains is supported by the experimental observation that the

backbone is locally coiled but persistent on larger length scales, just as in the simulation results of Saariaho and coworkers.

Their fourth effort [29] focussed on the influence of confinement on the conformational characteristics of comb copolymer brushes. The architecture under investigation consisted of a backbone of 100 segments to which 50 side chains were grafted with lengths up to 30 segments. All chains were flexible. The comb copolymer brush was confined between two impenetrable parallel plates. The spacing between the plates was varied between $Z = \infty$ (3D case) and $Z = 1$ (2D case). Interestingly, as the plates start squeezing together the brush as a whole starts to extend. However, whereas the radius of gyration of the side chains at a certain point starts decreasing and increasing again after a minimum has been reached, the radius of gyration of the backbone increases monotonically. Theory and simulations had previously shown isolated linear chains to have the same behavior as was observed here for the side chains. For 'soft' plates, theory predicted that the minimum would be smoothed out. As this was the kind of behavior that was observed for the backbone only the authors concluded that the presence of side chains effectively cushions the plates such that the backbone 'feels' soft plates.

The ratio λ/D was observed to increase considerably with decreasing plate separation. Moreover, it appeared to reach a maximum *before* the 2D situation was reached. When comparing the 2D and 3D case, a striking difference in behavior was observed. Whereas, as had previously been shown, for the 3D case the ratio λ/D levelled off at a certain side chain length the 2D case showed a linear increase with respect to side chain length after a length of 10 segments had been reached. The authors suggested that, as in the 2D case the scaling regime is reached for shorter chain lengths, for the 3D case the ratio λ/D may also increase for sufficiently large side chain lengths. This implies that lyotropic behavior due to intra-molecular excluded volume effects may be obtained for flexible polymers, which forms a strong incentive to investigate much larger systems.

In their final paper on the lyotropic behavior of bottle-brush molecules [30] Saariaho and coworkers introduced semi-flexible side chains. The intrinsic persistence of the side chains was varied by changing the characteristic angle between bonds in the freely jointed model that is employed. It was found that the persistence length of the comb copolymer increased

significantly when the rigidity of the side chains was increased and that the backbone becomes more extended at large length-scales. Also, the ratio λ/D was found to increase with side chain rigidity. The authors concluded that the semi-flexible nature of the side chains is of particular importance with respect to conformational elasticity and lyotropic behavior.

In 1999 Shiokawa and coworkers [33] published their work in which the scaling behavior of polymacromonomers was re-examined using the bond fluctuation method in good solvent. The length of the main chain as well as the side chains were varied up to 64 segments. The number of side chains was equal to the number of main chain segments, resulting in a very high grafting density. For short side chains it was observed that the comb copolymer behaves like a self-avoiding coil in three dimensions. As the length of the side chain increased the global shape of the main chain varied smoothly into an extended rod-like shape. The side chains were found to behave like self-avoiding coils in all situations, which is at variance with the results of Saariaho and coworkers [26, 27] and Rouault [25], but in agreement with the results of Gauger and Pakula [23] and Rouault and Borisov [24]. The authors suggested that the shape of the side chains depends on the degree of congestion of the elements and that further detailed studies are required to solve the discrepancy.

Khalatur and coworkers [34] reported on the conformational properties of molecular bottle-brushes in which a new algorithm was introduced. The results of this study however seem oddly at variance with the rest of the literature before and since the publication in 2000. Perfect self-avoiding walk statistics was found for comb copolymers consisting of a main chain of 30 segments and 30 side chains of length 6.

In the same year Khalatur and coworkers [35] published a study on molecular bottle-brushes in two dimensions. As has been discussed in chapter 1, experimentally strongly curved and helical structures had been observed by AFM of samples on mica. In their simulation study, a lattice model was used to simulate comb copolymer brushes with a frozen in asymmetric distribution of side chains with respect to both sides of the backbone. In agreement with experiment, of which some were also presented in the same paper, strongly helical shapes were reported even for a small asymmetry in the side chain distribution.

The influence of side chain length and side chain rigidity on the stiffness of ring comb copolymer brushes was investigated by Flikkema and coworkers [36]. It was found that with increasing side chain length the structure gradually stiffens, just as for the linear case, but that this effect stops to increase after the side chain length approaches the diameter of the ring at which a different regime is entered. Both flexible and rigid side chains were used and, as was reported by Saariaho and coworkers for linear chains, using rigid side chains was observed to be much more effective in obtaining a large persistence length. In addition, the presence of rigid side chains did not seem to influence the local backbone conformation.

At the beginning of the new millennium the focus of computer simulation studies on comb copolymer brushes seemed to shift from the investigation of conformational characteristics as a function of architecture and topology to the conformational properties as function of the chemical nature in terms of solvent quality and chemical (in)compatibility of different monomer types. The first such study to address intra-molecular microphase separation in comb copolymer brushes was reported by Vasilevskaya and coworkers [37]. The simulations were performed using the bond fluctuation model on a flexible comb copolymer with attractive interactions between monomer units of the side chains. Effectively, the side chains were experiencing solvent quality ranging from good solvent to very poor.

It was found that a sharp coil-to-globule transition takes place upon decreasing the solvent quality from good to poor solvent. In addition, the probability distribution of the radius of gyration shifts to lower values and becomes more narrow. In the region near the coil-to-globule transition the distribution exhibits two peaks, indicating a first order phase transition. When the solvent quality becomes poor beyond the coil-to-globule transition, the side chains organize themselves into micelles. For relatively short chains, the side chain material organizes into one micelle with the backbone material at the surface. As the length of the comb copolymer increases a critical micelle size is reached: The radius of the sphere reaches the point where it cannot increase without drawing in backbone material. This typically happens when the radius of the micelle becomes of the same magnitude as the average end to end point size of the side chains.

When increasing the length of the molecule even more, the aggregation of side chain material forms multiple micelles. Eventually, a cluster of micelles forms which is bound together and enveloped by backbone material.

in 2001 Timoshenko and coworkers [38] reported an off-lattice study on the equilibrium and kinetics at the coil-to-globule transition of star and comb heteropolymers in dilute solution. In this work a number of unusual conformational states and distinct folding pathways are reported that are strongly dependent on the macromolecular architecture.

The following year, Flikkema and coworkers [39] reported an off-lattice simulation study discussing the influence of side chain attraction on the conformational properties of two-dimensional polymer brushes with rigid side chains. When the backbone was rigid the side chains collapsed onto the backbone when a certain characteristic interaction strength was reached. For a flexible backbone it was observed that the persistence length of the backbone decreased with increasing side chain attraction, irrespective of whether the side chains were allowed to flip from one side to the other. When the side chains were allowed to flip the attraction between side chains caused aggregation of successive side chains at one side of the backbone. This resulted in a characteristic local spiralling of the backbone.

When the side chains were not allowed to flip, they were pointing alternatingly to opposite sides of the backbone. In this case, a plot of the bond-angle correlation function $\langle \cos\theta(s) \rangle$ showed a distinct odd-even effect, which is also observed in our study of 2D comb copolymers discussed in chapter 5 (see also [40]).

In 2004 Elli and coworkers [41] published a paper on the size and persistence length of molecular bottle-brushes. Backbone lengths up to 100 segments were considered and the conformational properties were compared to linear polymers. The simulations were performed for the athermal solvent regime. Their findings indicated that the size of the backbone for the branched systems is much larger than for their linear counterparts. In addition, the molecular size showed a power-law dependence on the backbone length with a swelling exponent that significantly exceeded those for linear chains. The authors note that they had some evidence that the results for the branched polymers were in a crossover region and that the SAW behavior for linear chains should be retained in the asymptotic limit of very long chains. In particular they pointed out that the persistence length

of the bottle-brushes, much larger than for linear chains, asymptotically increased with backbone length in the same way as for linear chains and that therefore it should eventually become independent of topology.

A determination of the probability distribution function for the backbone end-to-end distance showed a correlation hole effect that widened with side chain length, which is indicative of backbone stiffening. However, structure factor analysis showed that the scattering never reaches the rigid rod regime.

The authors remarked that the scaling exponent for the backbone size is in conflict with the results of Khalatur and coworkers [34]. Although they consider the possibility that the disagreement is due to lattice artifacts they do point out that their results *are* in agreement with the lattice simulation study of Shiokawa and coworkers [33]. In addition, the swelling exponents agree reasonably well with experimental values.

In the same year Sheng and coworkers [42] reported an off-lattice study discussing the effect of solvent quality on the conformations of comb copolymer brushes. In their paper the θ-temperature was first established by determining the temperature at which the second virial coefficient vanishes as well as the temperature at which the radius of gyration varies most rapidly with temperature. In the limit of infinite chains these temperatures coincide.

Structure factors of the backbone, the side chains and the whole polymer were determined. It was found that at the θ-temperature the structure factor of the whole polymer agrees well with the structure factor of Gaussian chains. At temperatures below the θ-temperature the polymers were found to collapse into approximately spherical conformations. The authors noted that the structure factor of the side chains indicated that these always remain in an expanded state, even in poor solvent, and attribute this effect to the strong interactions between side chains of densely branched systems. Using Kratky plots the authors showed that the side chains cause an increase of the rigidity of the comb copolymer as compared to linear polymers.

Connelly and coworkers [43] published an article on the difference between intrinsic and topological stiffness in branched polymers in 2005. The simulations were performed as off-lattice simulations. The systems under consideration were comb copolymer molecules with different grafting

density and side chain length, dendronized polymers with varying number of generations and linear polymers with intrinsic stiffness introduced by a bending potential.

It was found that the scattering behavior of linear polymers with intrinsic stiffness is substantially different from the scattering behavior of the backbone of topologically stiff branched polymers. At small length-scales the branched polymers appeared best modeled as semi-flexible polymers. However, for large length-scales the scattering behavior was more close to that of flexible polymers. The authors suggested that stiffness, in the case of branched polymers, is not uniform along the backbone. This was illustrated by an observable that indicates the stiffness depending on the position along the backbone via the projection of segment position vectors on the end-to-end vector. Comparison with intrinsically stiff polymers showed clear end effects for the branched polymers, i.e. the ends of the polymers were relatively flexible.

References

[1] D. Frenkel, B. Smit, "*Understanding molecular simulation: From algorithms to applications*", Academic Press, Inc., Orlando, FL, USA 1996.

[2] N. Metropolis, A. Rosenbluth, R. M.N., A. Teller, E. Teller, *J. Chem. Phys.* **1953**, *21*, 1087.

[3] J. de Jong, G. ten Brinke, *Macromol. Theory Simul.* **2004**, *13*, 318.

[4] Y. Tsukahara, K. Mizuno, A. Segawa, Y. Yamashita, *Macromolecules* **1989**, *22*, 1546.

[5] Y. Tsukahara, K. Tsutsumi, Y. Yamashita, *Macromolecules* **1989**, *22*, 2869.

[6] Y. Tsukahara, K. Tsutsumi, Y. Yamashita, S. Shimada, *Macromolecules* **1990**, *23*, 5201.

[7] B. Zimm, W. Stockmayer, *J. Chem. Phys.* **1949**, *17*, 1301.

[8] O. Ptitsyn, *J. Phys. Chem. USSR* **1955**, *29*, 396.

[9] A. Kron, O. Ptitsyn, *Vysokomolekul. Soedin.* **1963**, *5*, 397.

[10] G. Berry, O. T.A., *J. Chem. Phys.* **1963**, *40*, 1614.

[11] L. Gallacher, S. Windwer, *J. Chem. Phys.* **1966**, *44*, 1139.

[12] F. McCrackin, J. Mazur, *Macromolecules* **1981**, *14*, 1214.

[13] J. Lipson, S. Whittington, W. M.K., J. Martin, D. Gaunt, *J. Phys. A: Math. Gen.* **1985**, *18*, L469.

[14] W. M.K., D. Gaunt, J. Lipson, S. Whittington, *J. Phys. A: Math. Gen.* **1986**, *19*, 789.

[15] D. Gaunt, J. Lipson, S. Whittington, M. Wilkinson, *J. Phys. A: Math. Gen.* **1986**, *19*, L811.

[16] S. Whittington, J. Lipson, W. M.K., D. Gaunt, *Macromolecules* **1986**, *19*, 1241.

[17] J. Lipson, D. Gaunt, W. M.K., S. Whittington, *Macromolecules* **1987**, *20*, 186.

[18] M. Kosmas, D. Gaunt, S. Whittington, *J. Phys. A: Math. Gen.* **1989**, *22*, 5109.

[19] J. Lipson, *J. Comp. Chem.* **1987**, *8*, 333.

[20] M. Bishop, S. C.J., *J. Chem. Phys.* **1992**, *97*, 1471.

[21] M. Bishop, S. C.J., *J. Chem. Phys.* **1993**, *98*, 1611.

[22] J. Lipson, *Macromolecules* **1991**, *24*, 1327.

[23] A. Gauger, T. Pakula, *Macromolecules* **1995**, *28*, 190.

[24] Y. Rouault, O. V. Borisov, *Macromolecules* **1996**, *29*, 2605.

[25] Y. Rouault, *Macromol. Theory Simul.* **1998**, *7*, 359.

[26] M. Saariaho, O. Ikkala, I. Szleifer, I. Erukhimovich, G. ten Brinke, *J. Chem. Phys.* **1997**, *107*, 3267.

[27] M. Saariaho, I. Szleifer, O. Ikkala, G. ten Brinke, *Macromol. Theory Simul.* **1998**, *7*, 211.

[28] M. Saariaho, A. Subbotin, I. Szleifer, O. Ikkala, G. ten Brinke, *Macromolecules* **1999**, *32*, 4439.

[29] M. Saariaho, O. Ikkala, G. ten Brinke, *J. Chem. Phys.* **1999**, *110*, 1180.

[30] M. Saariaho, A. Subbotin, O. Ikkala, G. ten Brinke, *Macromol. Rapid. Commun.* **2000**, *21*, 110.

[31] G. Fredrickson, *Macromolecules* **1993**, *26*, 2825.

[32] T. Birshtein, O. Borisov, Y. Zhulina, A. Khokhlov, T. Yurasova, *Polymer Science USSR* **1987**, *29*, 1293.

[33] K. Shiokawa, K. Itoh, N. Nemoto, *J. Chem. Phys.* **1999**, *111*, 8165.

[34] P. G. Khalatur, D. G. Shirvanyanz, N. Y. Starovoitova, A. R. Khokhlov, *Macromol. Theory Simul.* **2000**, *9*, 141.

[35] P. G. Khalatur, A. R. Khokhlov, S. A. Prokhorova, S. S. Sheiko, M. Möller, P. Reineker, D. G. Shirvanyanz, N. Starovoitova, *Eur. Phys. J. E* **2000**, *1*, 99.

[36] E. Flikkema, A. Subbotin, G. ten Brinke, *J. Chem. Phys.* **2000**, *113*, 7646.

[37] V. V. Vasilevskaya, A. A. Klochkov, P. G. Khalatur, A. R. Khokhlov, G. ten Brinke, *Macromol. Theory Simul.* **2001**, *10*, 389.

[38] E. Timoshenko, Y. Kuznetsov, *Colloids and Surfaces A: Physicochem. Eng. Aspects* **2001**, *190*, 135.

[39] E. Flikkema, G. ten Brinke, *Macromol. Theory Simul.* **2002**, *11*, 777.

[40] J. de Jong, A. Subbotin, G. ten Brinke, *Macromolecules* **2005**, *38*, 6718.

[41] S. Elli, F. Ganazolli, E. Timoshenko, K. Y.A., R. Connolly, *J. Chem. Phys.* **2004**, *120*, 6257.

[42] Y.-J. Sheng, K.-L. Cheng, C.-C. Ho, *J. Chem. Phys.* **2004**, *121*, 1962.

[43] R. Connolly, B. Giovanni, E. Timoshenko, Y. Kuznetsov, S. Elli, G. F., *Macromolecules* **2005**, *38*, 5288.

Part II

Publications